FERMILAB-CONF-76-145-E E98

REVIEW OF ELECTRON AND MUON SCATTERING*

Luke W. Mo

Virginia Polytechnic Institute and State University

Blacksburg, Virginia 24061

Invited talk presented at the
Meeting of the Division of Particles and Fields,
American Physical Society,
Brookhaven National Laboratory
Upton, Long Island, New York
October 6-8, 1976

*Work supported by the National Science Foundation.

The scattering of high energy electrons from a nuclear target has become the classical method of studying the electromagnetic structure of nucleons.[1] In the energy range of hundreds of GeV, electrons are not readily available because of the enormous energy loss due to synchrotron radiation. Fortunately, muon beams from high energy proton accelerators can be used as an economic substitute to extend the kinematic range of investigations. It is well known that, to a high precision,[2] the muon and the electron have identical QED properties irrespective of their mass difference. They are equally effective in producing virtual photons which probe the target nucleon. In 1963, it was successfully demonstrated at BNL,[3] that a muon beam of reasonable intensity can be formed from the decay product of a focussed hadron beam of mainly pions; and it can be used for doing μp scattering experiments. In the last few years, experiments with muon beams of energies up to 300 GeV have been carried out at Fermilab. There has been much progress towards the understanding of the short-distance behavior of the nucleons. In this talk, I will try to summarize the new experimental results on the questions of scaling, nucleon structure functions, hadron distributions, and other related subjects in electron/muon scattering.

I. Elastic Scattering

Electron-proton elastic scattering was measured up to a q^2 value of 25 $(\mathrm{GeV}/c)^2$, where q^2 is the four-momentum transfer squared.[4] Electron-neutron elastic scattering,[5] using a deuterium target, was

measured only up to a q^2 value of approximately 6 $(GeV/c)^2$. The electric and magnetic form factors of the proton and the neutron are observed to obey the approximate "scaling" law:

$$G_E^p(q^2) = \frac{G_M^p(q^2)}{2.793} = \frac{G_M^n(q^2)}{-1.91} \simeq \frac{1}{(1 + \frac{q^2}{0.71})^2}$$

and

$$G_E^n(q^2) = 0 \quad .$$

The empirical form factor, $\frac{1}{(1 + q^2/0.71)^2}$, has been generally referred to as the "dipole" form factor. A detailed measurement at SLAC[4] revealed that the data differed from this numerical fit, even though it is a rather good approximation in general as shown in Figure 1. There were a great deal of theoretical effort in the past years trying to fit the data with vector dominance models. In 1974, asymptotically free gauge field theories were applied to predict the high-q^2 behavior of the magnetic form factor[6] by relating it to the deep inelastic structure functions. The calculations seem to agree well with the measured data.

Elastic μp scattering was first carried out at BNL.[3] Figure 2 shows the comparison between the μp and the ep elastic scattering data. They agree within experimental uncertainties. This measurement can be regarded as another proof of the "μe universality." Of course, it is more interesting to study the muon structure by comparing the ep and the μp scattering data. In Figure 2, the muon data appeared to be a little lower than the electron data. However, the systematic error

has prevented the possibility of a muon form factor as being significant.

II. Deep Inelastic Scattering

The cross section for the scattering of electrons of energy E to a final energy E' through an angle θ is related to the two inelastic form factors W_1 and W_2 by

$$\frac{d^2\sigma}{d\Omega dE'} = \frac{4\alpha^2}{q^4} \cos^2 \frac{\theta}{2} \left[W_2(q^2,\nu) + 2W_1(q^2,\nu)\tan^2 \frac{\theta}{2}\right] \quad ,$$

where $\nu = E - E'$ and $q^2 = 4EE'\sin^2 \frac{\theta}{2}$. The important discovery at SLAC, by an MIT-SLAC collaboration,[7] was that the two structure functions, νW_2 and $2MW_1$, are functions only of a single dimensionless variable $\omega = 2M\nu/q^2$, as shown in Figure 3. This is the celebrated Bjorken scaling.[8]

In order to explain Bjorken scaling, a great number of theoretical models were invented. Most of these theories point to the existence of constituents within nucleons. The parton model of Feynman is certainly the most popular version.[9] The other end of the spectrum includes the generalized vector dominance model;[10] or Schwinger's point of view[11] in which he believes the deep inelastic scattering phenomena can be explained by extrapolations from the known resonances production and diffraction scatterings. In the following sections, we will review the new experiment results on scaling, the inelastic structure function νW_2, and hadron spectra in electron/muon scattering. We hope that these experimental facts

can help us to understand the nucleon structure a little better; or at least to help us to decide which parts of the different theoretical models come closer to the truth.

III. Test of Bjorken Scaling

A Cornell-Michigan State-Berkeley-La Jolla collaboration has discovered at Fermilab that Bjorken scaling does not hold exactly.[12] In that experiment, the scale invariance was tested directly by comparing the invariant muon cross sections at different incident muon energies with the dimensions of the experimental apparatus properly scaled. Specifically, if the following scale transformation is made:

$E \rightarrow \lambda E$ (change the incident energy by a factor of λ),

$E' \rightarrow \lambda E'$ (change the magnetic spectrometer setting by a factor of λ),

$\theta \rightarrow \frac{1}{\sqrt{\lambda}}$ (change the target to spectrometer distance by a factor of $\frac{1}{\sqrt{\lambda}}$)

then the Bjorken scaling variable ω will remain unchanged and the ratio of the cross sections at two different incident energies, defined by

$$r(\omega,q^2) \equiv \frac{[E \frac{d^2\sigma}{dxdy}]_{E = \lambda E_0}}{[E \frac{d^2\sigma}{dxdy}]_{E = E_0}} ,$$

where $x = q^2/2M\nu$, $y = E'/E$, will remain constant for all values of ω and q^2 if Bjorken scaling holds strictly true. The experimental results, measured at incident muon energies of 150 GeV and 56 GeV with

an iron target, is shown in Figure 4. It clearly demonstrates that the Bjorken scaling is violated by ∿20%. The same group also compared their measured data to a Monte Carlo calculation in which Bjorken scaling was assumed. This result is shown in Figure 5. The plot explicitly illustrates the q^2 dependence of scaling violation at different values of ω. The deviation from Bjorken scaling as a function of q^2 has a negative slope at values of ω less than 5; and a positive slope at values of ω greater than 5. This observation is in good agreement with the theoretical predictions of both conventional field theories and also asymptotically free gauge theories with anomalous dimensions.[13,14]

In another experiment at Fermilab, done by a Chicago-Harvard-Illinois-Oxford collaboration,[15] the structure function, νW_2, was directly measured by scattering 150 muons from a liquid hydrogen or deuterium target. The result is shown in Figure 6. It demonstrates also that Bjorken scaling is violated by an amount less than 20%, and is consistent with the results of Reference 12.

One very important question about scaling is what should be the correct scaling variable.[16] There exist already too many of them such as x, x', x_S, x_J, x_ψ, ξ, etc. The argument is that the energy reached by various experiments is still too low to be free of corrections due to kinematics or the masses of the constituents. This difficulty is vividly illustrated by a recent precise measurement at SLAC with 20 GeV electrons.[17] As shown in Figure 7, at high q^2 values the structure function $2MW_1$ does not scale with either the Feynman variable or the Bloom-Gilman variable x'. However, it scales

rather well with a specially chosen empirical variable defined by $x_s \equiv q^2/(2M\nu + 1.48)$. For the hundred GeV muon energies at Fermilab, the quantity $2M\nu$ is of the order of 300. The scaling variables defined by various authors become approximately identical and the observed deviations from scaling cannot be eliminated by a particular choice of the scaling variable.

At high values of ν and q^2, it is anticipated that new degrees of freedom of the nucleon can be excited.[18,19] For example, heavy quark excitations could manifest threshold effects in νW_2; and color excitation could manifest as a general increase of νW_2. None of these effects have been observed.

IV. Approach to Scaling

Facing the fact that the exact Bjorken scaling has not yet been reached, the natural question to ask is how scaling is approached as a function of q^2 and ν. In Figure 8, the νW_2 function measured at SLAC[20] with 20 GeV electrons is plotted against q^2 for all values of ω'. It can be seen that νW_2 approaches the scaling limit ($\sim 1/\pi$) when $q^2 \gtrsim 1.2\ (\mathrm{GeV}/c)^2$. In Figure 9, a similar plot is shown for data measured in 150 GeV μD scattering at Fermilab.[21] The structure function only starts to level off at $q^2 \simeq 3.5\ (\mathrm{GeV}/c)^2$, instead of the value of $q^2 \simeq 1.2\ (\mathrm{GeV}/c)^2$ as shown in Figure 8. This phenomena was independently confirmed by the results of scattering 150 GeV muons from an iron target[22] as shown in Figure 10. Apparently a ν-dependence of the structure function νW has been observed. As ν is increased from 20 GeV to 150 GeV, it takes higher values of q^2 to reach the scaling limit.

As we have mentioned before, asymptotically free gauge theories[13] seem to be able to account for the observed deviation from scaling. The explanation is somewhat complicated. A very appealing and intuitive picture has been discussed informally by Wilson.[23] The argument is based on analogy with the electron bremsstrahlung process. As is well known, if the radiative corrections were not taken into account, the Bjorken scaling will be violated by 50% or more. From the measured νW_2 function, it has been realized that approximately 50% of the momentum imparted to the nucleon by the virtual photon is missing. These missing momenta are supposedly taken away by the inert neutral gluons. If the quark-parton model, as pictured in Figure 11, is to be taken seriously, then Wilson[23] argued that gluon emissions by the quarks should also be corrected as what was done with the photon emissions by the electrons. Then we may end up with a perfect Bjorken scaling after all. It is the gluon emission processes which give rise to the present scaling violation as shown in Figure 12. Presumably the gluon emission processes can be calculated once the quark-gluon coupling constant, $g/4\pi$, is known. This coupling constant can be calculated from the slope of the plot of $\frac{\partial \ln F(\omega,q^2)}{\partial \ln q^2}$ vs. ω, according to Tung,[24] as shown in Figure 13.

V. The νW_2 Function

In Figure 14, the result on νW_2 is shown as a function of x from the data of scattering 150 GeV muons from a liquid deuterium target at Fermilab.[13] The salient feature of this plot is that νW_2 decreases at small values of x. A similar result, as shown in Figure 15, was also observed at BNL by scattering $\sim$7 GeV muons from a copper target.[25]

The decrease of νW_2 at small x is predicted by a few specific models, using valence quarks and an infinite sea of quark-antiquark pairs, as suggested by Kuti and Weisskopf,[26] Landshoff and Polkinghorne,[27] and by Altarelli et al.[28] Regge-pole models can also predict the same behavior.[29]

It is important to know the x-distributions of the quark or the antiquark components of the nucleon. This information has profound bearing in designing future colliding beam facilities to study the production of the W-bosons. For example, one can estimate the W-boson production cross section by assuming the $q\bar{q}$ annihilation mechanism as suggested by Drell and Yan.[30] Figure 16 shows the valence quark and sea quark distributions as resolved by Barger et al.[31] using a quark-parton model. The $\bar{q}$-component was found to be approximately 6%. This is in agreement with the results of a neutrino scattering experiment[32] at Fermilab.

VI. The Shadowing Effect

It is well known that the A-dependence of the total hadronic cross sections in real photon-nucleus collisions is proportional to $A^{1-\epsilon}$ rather than A.[33] This is called the "shadowing" effect. However, for interactions of virtual photons with complex nuclei this shadowing effect was not observed.[34] The results are illustrated in Figure 17.[35] The situation is quite puzzling. It has been anticipated in the generalized vector dominance model that the photon should contain hadronic components, which lead to this shadowing effect. It is difficult to understand why the shadowing effect disappears as soon as the

photon becomes virtual. As shown in Figure 17, the predictions of the generalized vector dominance model completely fail for electroproduction even though it enjoys success in some other areas.

An experiment at Cornell[36] has demonstrated the existence of a shadowing effect of approximated 20% in electroproduction as shown in Figure 18. However, this result was not reproduced in a more recent BNL muon scattering experiment[37] as shown in Figure 19.

VII. Interference Effect Between Electromagnetic and Weak Interactions

Electron/muon scattering also offers an opportunity to study the neutral current in weak interactions by observing the interference effect of its amplitude

$$\frac{G_o}{\sqrt{2}} \langle e' | \gamma_\mu (1 + \gamma_5) | e \rangle J_\mu^{hadron} \quad ,$$

where G_o is a constant to be determined, with that of one-photon exchange in electromagnetic interactions,

$$4\pi\alpha \langle e' | \gamma_\mu | e \rangle \frac{1}{q^2} J_\mu^{hadron} \quad .$$

The cross section is estimated to be[38]

$$\frac{d^2\sigma}{dq^2 d\nu} = \left(\frac{d^2\sigma}{dq^2 d\nu}\right)_{E.M.} \left[1 + P(2 \text{ to } 4) \times 10^{-4} q^2 \left(\frac{G_o}{G_F}\right)\right]$$

where P is the longitudinal beam polarization; G_F, the Fermi coupling constant, $10^{-5}/M_p{}^2$; and q^2, the four-momentum squared in $(GeV/c)^2$. The

quantity measured in the experiment is defined by the asymmetry,

$$A = \frac{\sigma(+) - \sigma(-)}{\sigma(+) + \sigma(-)}$$

where σ is the cross section $d^2\sigma/dq^2d\nu$; and $(\pm)$ represents the beam helicity. From the simple form of the neutral current amplitude assumed, the asymmetry has the value

$$A = (2 \text{ to } 4) \times 10^{-4} q^2 P(G_O/G_F) \quad .$$

If we assume a different form of interactions given by the neutral currents of the Weinberg-Salam model, the values of A can be an order of magnitude smaller depending on the value of the parameter $\sin^2\theta_W$, where θ_W is the Weinberg angle.

Since the muon beam is produced mainly from the decay of pions, it is longitudinally polarized. The sign and magnitude of the muon polarization can be selected by choosing the muon energy for a pion beam of fixed energy. An experiment of scattering muons in the energy range of 15 to 27 GeV was performed at Serpukhov, U.S.S.R.[39] The result is negative and the upper limit is given as

$$G_O = (-4 \pm 12)G_F \ .$$

Recently high energy polarized electrons were made available at SLAC by a Yale-SLAC collaboration.[40] The longitudinally polarized electrons were first produced from photoionization of polarized Li^6 atoms, and then accelerated to energies up to 19.4 GeV with negligible

depolarization. Asymmetry was measured on the polarized electrons scattered from an unpolarized deuterium target. The parameters of the experiment are given in Table 1. The statistical accuracy is $\Delta G_0 = \pm 1.9\ G_F$ at $q^2 = 1.2\ (\mathrm{GeV}/c)^2$; and $\Delta G_0 = \pm 5.1\ G_F$ at $q^2 = 4.2\ (\mathrm{GeV}/c)^2$. The dominant systematic uncertainty is from the energy imbalance (at the level of 10^{-4}) between the two beam polarizations. This energy imbalance yields an error of $\Delta G_0 \simeq 10\ G_F$. The final result is given as

$$G_0 \lesssim 10\ G_F \quad .$$

VIII. The Final-State Hadron Distributions

It is the hope that the deep inelastic scattering phenomena can be understood if we have complete measurements of the final-state hadrons. The space-like virtual photon has the peculiar property that it carries more momentum than energy. Therefore, it cannot fragment into hadrons by itself. When the virtual photon collides with the target nucleon, it will transfer the three-momentum to a single quark within the nucleon which will subsequently fragment into ordinary hadrons. Therefore, study of the final-state hadrons in electro- or muo-production could offer a direct opportunity to understand the nucleon structure. As the q^2 values continue to increase, eventually we hope that the quarks can be ejected free from the nucleon even though the present theories all call for the confinement of quarks.

A. The $x_{\parallel}$-Distribution

The $x_{\parallel}$-distribution in a 150 GeV μD scattering experiment[15,21,41] at Fermilab is shown in Figure 20, where $x_{\parallel}$ is the Feynman variable defined as $x_{\parallel} \equiv P_{\parallel}/P_{max}$; $P_{\parallel}$ is the longitudinal component of the hadron

momentum along the photon direction, and P_{max} is the maximum hadron momentum in the photon-nucleon C.M. system.

In Figure 21, the z-distributions of hadrons produced in e^+e^- annihilations at SPEAR of SLAC[42] are shown, where $z \equiv x_{\parallel}$. In Figure 22, the x-distribution for hadrons produced by neutrinos in the 15' bubble chamber at Fermilab[43] is shown. In both Figures 21 and 22, the solid lines are the results from muoproduction. By comparing these results, it is most interesting to notice that the hadron distributions are identical in interactions with space-like photons, time-like photons, and neutrinos. This observation provides strong support for the constituent models of nucleon structure. Similar results at SLAC were also published by a SLAC-UC/Santa Cruz collaboration.[44]

B. The Charge Ratio

The charge ratios, N_{h^+}/N_{h^-} and N_{π^+}/N_{π^-}, measured at SLAC by an MIT-SLAC collaboration[45] with good Cherenkov identification, are shown in Figure 23 as functions of q^2. The targets were liquid hydrogen and deuterium. The data for the neutron were obtained by subtraction.

Also, in the same electroproduction experiment, the kaon and antiproton components were measured to be $N_k/N_\pi \simeq 10\%$ and $N_{\bar{p}}/N_\pi \simeq 1\%$. The production of kaons contradicts a prediction by K. Wilson[46] which anticipates approximately 50% of hadrons are kaons.

C. The x_T-Distribution

It was found that in pp collisions, at ISR of CERN and at Fermilab,[47] the invariant cross sections for observing a single pion can be parameterized in the following form:

$$E \frac{d^3\sigma}{d\vec{p}^3} = f(x_T)/W^n$$

where $x_T \equiv P_T/P_{max}$ in the C.M. system, W is the C.M. energy, and n is an empirical constant and found to be between 8 to 11. If this scaling law in x_T also holds in virtual photoproduction, then the quark-parton model can be regarded as more fundamental than we expected.

A Cornell-Harvard collaboration[48] has measured the π^+ inclusive cross sections in the reaction $\gamma_V + p \to \pi^+ +$ anything. The results are shown in Figure 24. At fixed values of q^2, the ratio of the invariant cross section, $Ed^3\sigma/d^3\vec{p}$ to the total virtual photoproduction cross section, σ_T, does not scale in x_T. It decreases more rapidly for higher values of W. Figure 25 shows the value of n. It varies over a much wider range than in pp collisions.

IX. The Future Outlook

μp or ep scattering experiments are rather difficult experimental undertakings as compared to hadron-hadron scattering experiments. However, the experimental results are relatively easier to interpret because only one hadron is involved in the initial state. It is stimulating to see that there are many experiments being carried out/or planned in this field. In particular, a muon beam of intensity 10^9/pulse is expected to operate at the SPS at CERN within a year. Two large-scale muon scattering spectrometers are currently under construction. Also, we anticipate new results from the following experiments currently in progress or in the planning stage:

A. The Exclusive Channels

An electroproduction experiment[49] at Cornell is due to complete shortly. The apparatus consists of a magnetic spectrometer equipped with a large number of arrays of MWPC's. The experiment will yield high statistics results on vector meson and resonance production. Some typical raw data are shown in Figures 26 through 28.

B. The Nuclear Emulsion Experiment

A Cornell-Europe-Fermilab-Seattle collaboration[50] has finished the running of a charm search experiment with nuclear emulsions at Fermilab. The ingenious feature of this investigation is that it is an electronically triggered experiment. Stacks of nuclear emulsions are placed in front of a toroidal magnetic muon scattering spectrometer. The nuclear emulsions are sandwiched between two sets of high-resolution drift wire chambers. Upon occurrence of a muon scattering trigger, the interaction vertex can be located by the drift chambers to the accuracy of $\lesssim 150\ \mu$. This will greatly reduce the scanning time. The high resolution of the nuclear emulsion will permit the detection of short-lived charmed particles to a high precision.

C. Tri-Muon Experiment

A Michigan State University group[51] has finished the running of a tri-muon search experiment at Fermilab with muons at energies of up to 270 GeV. The reaction under investigation is

$$\mu^+ + A \rightarrow \mu^{+'} + C + \bar{C} + X$$

$$\bar{C} \rightarrow \mu^- + \ldots$$

$$C \rightarrow \mu^+ + \ldots$$

where C and $\bar{C}$ denote the charmed and the anti-charmed states. The extra muon-pair could also originate from the production of heavy lepton-pairs. Presumably the $C\bar{C}$ production rate can be related to that observed in neutrino interactions at Fermilab through the use of CVC theorem.

D. ep Colliding Beam Facility

Thus far the maximum q^2 value reached in electron/muon scattering experiments is only about 50 $(GeV/c)^2$, and the maximum ν value is less than 300 GeV. It is difficult to see how these numbers can be increased by more than a factor of four in the future for fixed target accelerators. The most effective way to increase the q^2 and ν limits is by an ep colliding beam facility, first suggested at SLAC.[52] The ep colliding beam facility would provide the opportunity to study both the electromagnetic and weak interactions. The strengths of the electromagnetic and weak interactions are comparable when

$$\frac{G_F{}^2 S}{\pi} = \frac{4\pi\alpha^2}{S}$$

or when S = 4,000 GeV^2, where S is the C.M. energy squared. Beyond this S value, the weak interaction process $e + p \rightarrow \nu_e + X$ will dominate. This neutrino inclusive reaction offers the best opportunity to study the production of W-bosons. In the old Fermi theory of weak interactions, the cross section for the process $e + p \rightarrow \nu_e + X$ is proportional to S. If W-bosons exist, the cross section will be modified by the propagation factor $1/(1 + q^2/M_W{}^2)^2$, where M_W is the mass of the intermediate boson. If M_W is $\sim$100 GeV or larger, the deviation from a linear

rise of the cross section with respect to S can be easily detected if $q^2 \gtrsim M_W^2$. This high value of q^2 can only be reached with ep colliding beams.

There have been many studies on ep colliding beam facilities. Recently, this subject was rediscussed at the 1976 Fermilab Summer Study.[53] It was found that a 20 GeV electron storage ring can be built fairly economically at Fermilab by placing it inside the main ring tunnel. Since the radius of the proton synchrotron is 1 km, the magnetic field required for 20 GeV electrons is only 670 gauss and the energy losses due to synchrotron radiation are quite moderate. If this 20 GeV electron is allowed to collide with the 1,000 GeV protons in the future Energy Doubler, the q^2 and ν limits can be extended to 80,000 $(\mathrm{GeV}/c)^2$ and 40,000 GeV respectively. The estimated counting rate for deep inelastic electrpn-proton scattering is shown in Figure 29. The counting rate for weak interactions, assuming the Fermi theory, is shown in Figure 30.

X. Acknowledgment

I wish to express my sincere thanks to Prof. L. N. Hand, Dr. R. H. Heisterberg, Dr. J. Martin, Prof. A. C. Melissinos, Prof. M. L. Perl, Prof. F. M. Pipkin, and Prof. R. E. Taylor for discussions and help in preparing this talk.

REFERENCES

1. R. Hofstadter, Electron Scattering and Nuclear and Nucleon Structure, W.A. Benjamin, New York (1963).

2. F. H. Combley, Proceedings of the 1975 International Symposium on Lepton and Photon Interactions at High Energies, W. R. Kirk, ed., Stanford University, Stanford, California (1975), p. 913.

   B. L. Beron et al., Phys. Rev. Letters 33, 663 (1974).

3. A. Entenberg et al., Phys. Rev. Letters 32, 486 (1974).

4. D. H. Coward et al., Phys. Rev. Letters 20, 292 (1968).

   P. N. Kirk et al., Phys. Rev. D8, 63 (1973).

5. P. Stein et al., Phys. Rev. Letters 16, 592 (1966).

   R. H. Budnitz et al., Phys. Rev. 173, 1359 (1968).

6. D. J. Gross and S. B. Treiman, Phys. Rev. Letters 32, 1145 (1974).

   A. De Rujula, Phys. Rev. Letters 32, 1143 (1974).

7. W. K. H. Panofsky, Proceedings of the XIV International Conference on High Energy Physics, J. Prentki and J. Steinberger, eds., CERN, Geneva, Switzerland (1968), p. 23.

   M. Breidenbach et al., Phys. Rev. Letters 23, 935 (1969).

8. J. D. Bjorken, Proceedings of the International School of Physics, "Enrico Fermi" Course XLI, J. Steinberger, ed., Academic Press, New York (1968).

9. R. P. Feynman, Photon-Hadron Interactions, W.A. Benjamin, Inc., Reading, Massachusetts (1972).

10. J. J. Sakurai and D. Schildknecht, Phys. Letters 40B, 121 (1972); 41B, 489 (1972); 42B, 216 (1972).

    K. Fujikawa, Phys. Rev. D9, 2794 (1971).

11. J. Schwinger, Proc. Nat. Acad. Sci., U.S.A., Vol. 72, No. 1, January 1975, p. 1; also Vol. 73, 1976.

12. Y. Watanabe et al., Phys. Rev. Letters 35, 898 (1975).

C. Chang et al., Phys. Rev. Letters 35, 901 (1975).

13. Wu-ki Tung, Phys. Rev. Letters 35, 490 (1975); Phys. Rev. D12, 3613 (1975).

14. H. Georgi and H. D. Politzer, Phys. Rev. Letters 36, 1281 (1976).

15. H. L. Anderson et al., Phys. Rev. Letters 36, 1422 (1976).

L. W. Mo, Proceedings of the 1975 International Symposium on Lepton and Photon Interactions at High Energies, W. R. Kirk, ed., Stanford University, Stanford, California (1975), p. 651.

16. R. Barberi, J. Ellis, M. K. Gallard, and G. G. Ross, CERN Report CERN.TH.2192 (1976).

17. W. B. Atwood et al., SLAC Report SLAC-PUB-1758, Stanford Linear Accelerator Center, Stanford University, Stanford, California (1976).

18. Y. Nambu and M. Y. Han, Phys. Rev. D10, 674 (1974).

19. J. C. Pati and A. Salam, Phys. Rev. Letters 36, 11 (1976).

20. S. Stein et al., Phys. Rev. D12, 1884 (1975).

21. R. H. Heisterberg, Ph.D. Thesis, University of Chicago, 1976 (unpublished).

22. L. N. Hand, private communication.

23. Robert R. Wilson, private communication.

24. Wu-ki Tung, preprint, Illinois Institute of Technology, Chicago, Illinois (1976).

25. A. Melissinos, private communication. The author is most grateful to the BNL-Rochester-NSF collaboration for making their preliminary data available to this Conference.

26. J. Kuti and V. F. Weisskopf, Phys. Rev. D4, 3418 (1971).

27. P. V. Landshoff and J. C. Polkinghorne, Nucl. Phys. 28, 240 (1971); Phys. Rev. D8, 4157 (1973).

28. G. Altarelli, N. Cabibbo, L. Maiani and R. Petronzio, Nucl. Phys. B69, 531 (1974).

29. F. E. Close and J. F. Gunion, Phys. Rev. D4, 742 (1971).

30. S. D. Drell and T. M. Yan, Phys. Rev. Letters 25, 316 (1970).

31. V. Barger, private communication.

V. Barger and R. J. N. Phillips, Nucl. Phys. B73, 269 (1974).

32. A. Benvenuti et al., Phys. Rev. Letters 36, 1478 (1976).

33. D. O. Caldwell et al., Phys. Rev. Letters 23, 1256 (1969); 25, 796 (1970).

34. H. W. Kendall, Proceedings of the 5th International Symposium on Electron and Photon Interactions at High Energies, Cornell University, Ithaca, New York (1971); also see Reference 20.

35. J. J. Sakurai, Proceedings of the International School of Subnuclear Physics, Erice, Sicily, Italy (1973).

36. J. Eickmeyer et al., Phys. Rev. Letters 36, 289 (1976).

37. A. Melissinos, private communication.

38. E. Derman, Phys. Rev. D7, 2755 (1973); S. M. Berman and J. R. Primack, Phys. Rev. D9, 2171 (1974).

39. Yu. B. Bushnin et al., Phys. Letters 64B, 102 (1976).

40. C. Y. Prescott et al., SLAC preprint (1976), private communication by Prof. R. E. Taylor.

41. W. A. Loomis et al., Phys. Rev. Letters 35, 1483 (1975).

42. M. L. Perl, SLAC Report SLAC-PUB-1614, Stanford Linear Accelerator Center, Stanford University, Stanford, California (1971).

43. J. P. Berge et al., Fermilab preprint, Batavia, Illinois (1975).

44. K. Bunnell et al., Phys. Rev. Letters 36, 772 (1976).

45. J. F. Martin et al., SLAC Report SLAC-PUB-1766, Stanford Linear Accelerator Center, Stanford University, Stanford, California (1971).

46. K. G. Wilson, Phys. Rev. Letters 27, 690 (1971).

47. F. W. Busser et al., Phys. Letters 46B, 471 (1973).

J. W. Cronin et al., Phys. Rev. D11, 3105 (1975).

48. A. Browman et al., Phys. Rev. Letters 37, 651 (1976).

49. H. White, private communication.

50. L. N. Hand et al., private communication.

51. W. Chen et al., private communication.

52. Particle Physics with Positron-Electron-Proton Colliding Beams, SLAC Report SLAC-146, LBL-750, UC-34 (1972).

53. D. Berley, P. J. Limon, L. W. Mo, A. L. Read and R. J. Stefanski, Fermilab 1976 Summer Study.

Table I

Polarized Electron Source-Photoionization of polarized Li^6 atomic beam	
180 pulses per second	1.5 μsec pulse length
1.2×10^9 e^-/pulse on target	50 ± 6% polarization
5×10^7 pulses accumulated	
Flux on target - 6×10^{16} e^-	Polarization reversal ∿every 2 minutes
Kinematic Points-E_0 = 19.4 GeV	
20-GeV/c spectrometer	8-GeV/c spectrometer
$\theta = 3.5°$	$\theta = 13.3°$
p = 16.5 GeV/c momentum	p = 4.0 GeV/c momentum
$Q^2 = 1.2$ GeV/c^2	$Q^2 = 4.2$ GeV/c^2
W = 2.3 GeV	W = 5.1 GeV
$\omega = 4.6$	$\omega = 6.9$
$\nu = 2.9$ GeV	$\nu = 15.4$ GeV

FIGURE CAPTIONS

Figure 1 The ratio of ep elastic scattering cross section measured at SLAC to that calculated with the dipole form factor.

Figure 2 Comparison of ep and μp elastic scattering cross sections. The μp scattering data are from several experiments at BNL.

Figure 3 The inelastic proton structure function measured at SLAC as a function of the Bjorken scaling variable ω.

Figure 4 Comparison of 150 GeV and 56 GeV muon scattering from an iron target. The quantity V is defined as $V = q^2/2ME$.

Figure 5 Comparison of the muon-iron scattering data to a Monte Carlo calculation using scale-invariant form factors.

Figure 6 The q^2-dependence of νW_2 for different ranges of ω.

Figure 7 This figure illustrates the scaling (or nonscaling) behavior of $2MW_1$ for various scaling variables. The average value of $2MW_1$ in the x or x' or x_S range from 0.6 to 0.7 is evaluated at a value of the scaling variables of 0.65 and is plotted as a function of Q^2. For x and x', $2MW_1$ decreases as Q^2 increases, indicating a breakdown of scaling in these variables. For x_S the data are consistent with scaling.

Figure 8 νW_2 measured at SLAC as a function of q^2 for all values of ω'. The curve is a fit by J. Schwinger, $\frac{1}{\pi} \frac{q^2}{q^2 + 0.36}$.

Figure 9 νW_2 as a function of q^2 for data in the range $90 \leq \nu \leq 130$ GeV.

Figure 10 νW_2 as a function of q^2 for all values of ω. The data was measured at Fermilab by scattering muons from an iron target.

Figure 11 Inelastic electron scattering in the parton model.

Figure 12 Photon emissions and gluon emissions in electron-quark inelastic scattering. The gluon-quark coupling constant is $g/4\pi$.

Figure 13 Comparison of experimentally observed scaling violation with that anticipated from asymptotically free color gauge theory. $F(\omega,q^2)$ is νW_2. The slope is equal to $(g/4\pi)^2$, the gluon-quark coupling squared.

Figure 14 νW_2 as a function of the Feynman scaling variable $x = q^2/2M\nu$ measured at Fermilab.

Figure 15 νW_2 as a function of x', where $x' = q^2/(2M\nu + M^2)$. The data is from muon-copper scattering measured at BNL.

Figure 16 A parton model fit to the μD data by Barger, showing the relative contributions of the valence quarks and the sea of $q\bar{q}$ pairs.

Figure 17 Shadowing effect in photoproduction and electroproduction. This figure is taken from Ref. 35. The curves are predictions of generalized vector dominance model with q^2 values indicated.

Figure 18 A_{eff}/A measured with electron scattering from C and Ta. Curves are calculations of Spital and Yennie with a vector dominance model.

Figure 19 Preliminary data on A-dependence of muon scattering at BNL. No shadowing effect was seen.

Figure 20 The $x_{\parallel}$-distribution for hadrons produced in the kinematic region $1 \leq q^2 \leq 10\ (\mathrm{GeV}/c)^2$ and $90 \leq \nu \leq 130$ GeV.

Figure 21 The z-distribution of hadrons produced by e^+e^- annihilations at SPEAR. The straight line is the numerical fit of the muoproduction data shown in Figure 20.

Figure 22 The z-distribution of the hadrons produced by neutrino interactions at Fermilab. The straight line is the numerical fit of the muoproduction data shown in Figure 20.

Figure 23 The positive-to-negative charge ratios as functions of q^2 measured at SLAC. The solid points are for N_h+/N_h-, the open circles are for $N_\pi+/N_\pi-$.

Figure 24 Plots of the invariant structure function $\frac{1}{\sigma_T} E \frac{d^3\sigma}{d\vec{p}^3}$ vs. the scaling variable x_T.

Figure 25 A plot of the fit parameter n vs. x_T for electroproduction of π^+.

Figure 26 $\pi\pi\pi^\circ$ invariant mass plot of an electroproduction experiment at Cornell University.

Figure 27 Invariant mass plot of $\pi^+\pi^-$ and π^+p events of an electroproduction experiment at Cornell University.

Figure 28 Invariant mass plot of Kp events of an electroproduction experiment at Cornell University.

Figure 29 Deep inelastic ep scattering event rate assuming:

(1) $\nu W_2 \simeq (1 - x)/4$ and $W_1/W_2 \simeq \nu^2/q^2$,

(2) 100% detection efficiency.

Figure 30 Weak interaction event rate for spin 1/2 parton model assuming:

(1) $\sigma_{\nu N}^{total} = 8 \times 10^{-39} \nu_{max}$ cm^2,

(2) $\nu W_2 \propto (1 - x)$,

(3) $\sigma_R = \sigma_S = 0$,

(4) 100% detection efficiency.

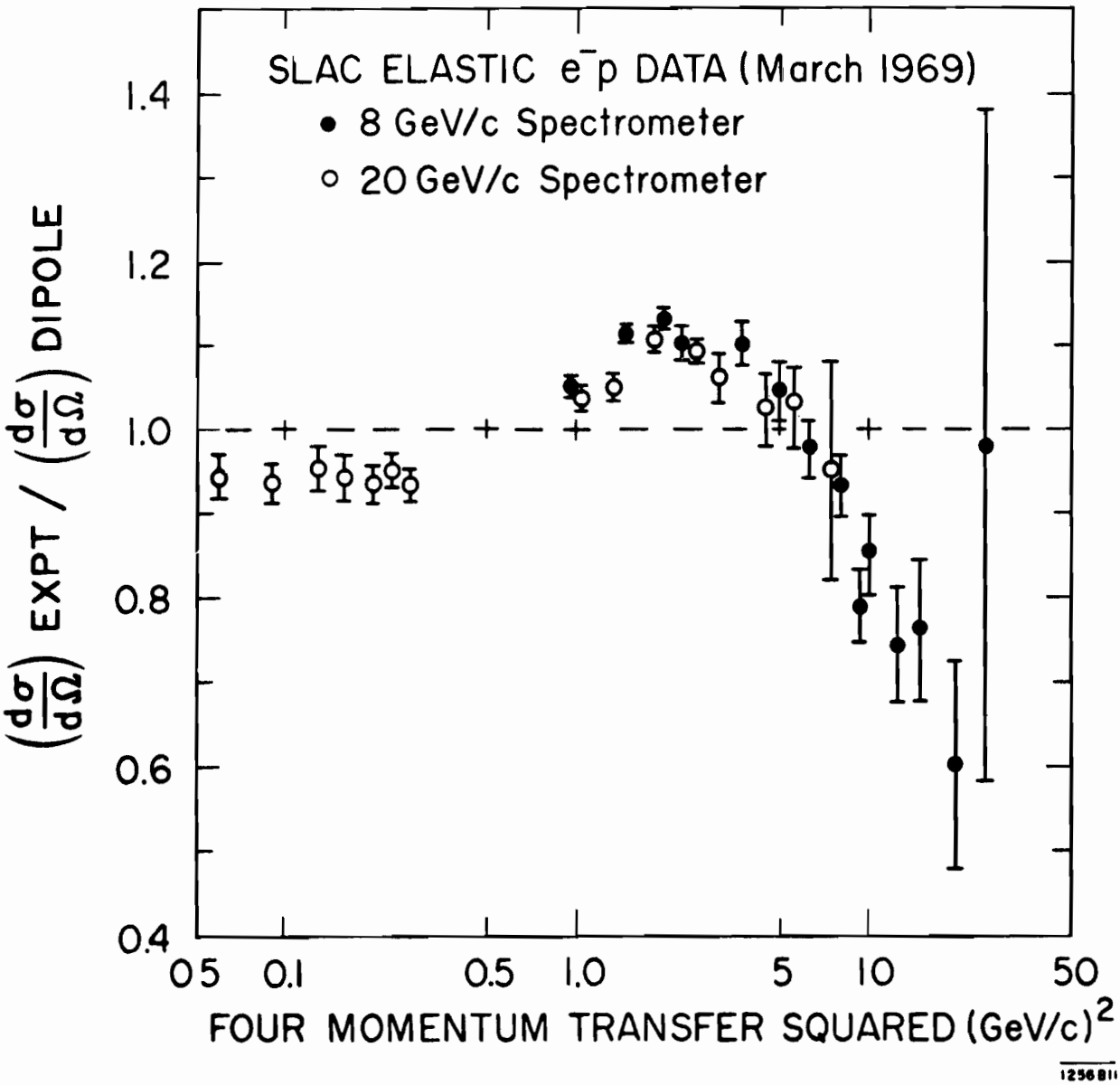
SLAC ELASTIC e⁻p DATA (March 1969)
• 8 GeV/c Spectrometer
○ 20 GeV/c Spectrometer
(dσ/dΩ) EXPT / (dσ/dΩ) DIPOLE
1.4
1.2
1.0
0.8
0.6
0.4
0.5
0.1
0.5
1.0
5
10
50
FOUR MOMENTUM TRANSFER SQUARED (GeV/c)²
1256B11

Figure 1

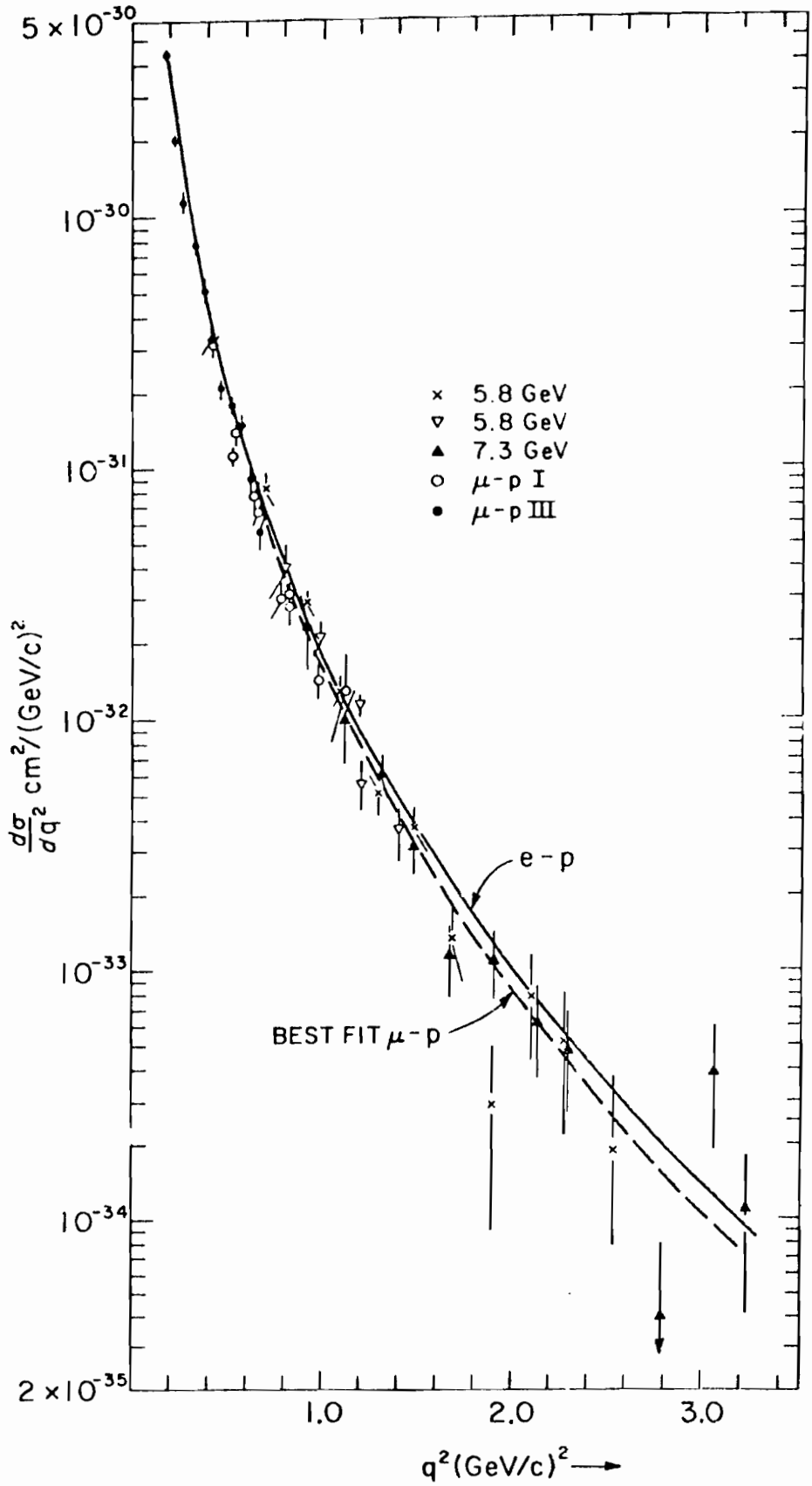
5 × 10^-30
10^-30
10^-31
10^-32
10^-33
10^-34
2 × 10^-35
dσ/dq² cm²/(GeV/c)²
× 5.8 GeV
▽ 5.8 GeV
▲ 7.3 GeV
○ μ-p I
● μ-p III
e - p
BEST FIT μ-p
1.0
2.0
3.0
q²(GeV/c)²

Figure 2

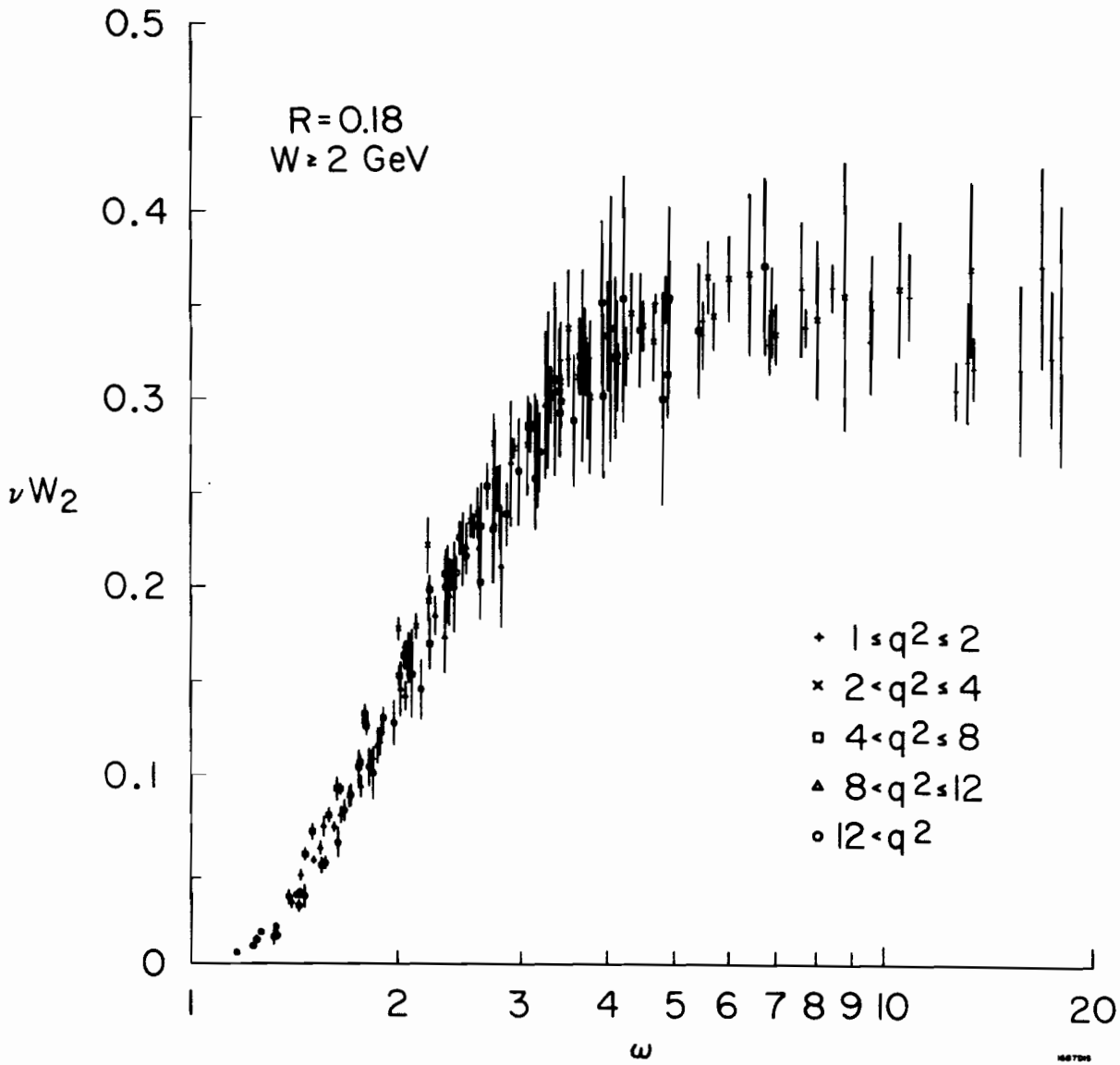
R = 0.18
W ≥ 2 GeV
0.5
0.4
0.3
0.2
0.1
0
νW_2
1
2
3
4
5
6
7
8
9
10
20
ω
$1 \le q^2 \le 2$
$2 < q^2 \le 4$
$4 < q^2 \le 8$
$8 < q^2 \le 12$
$12 < q^2$

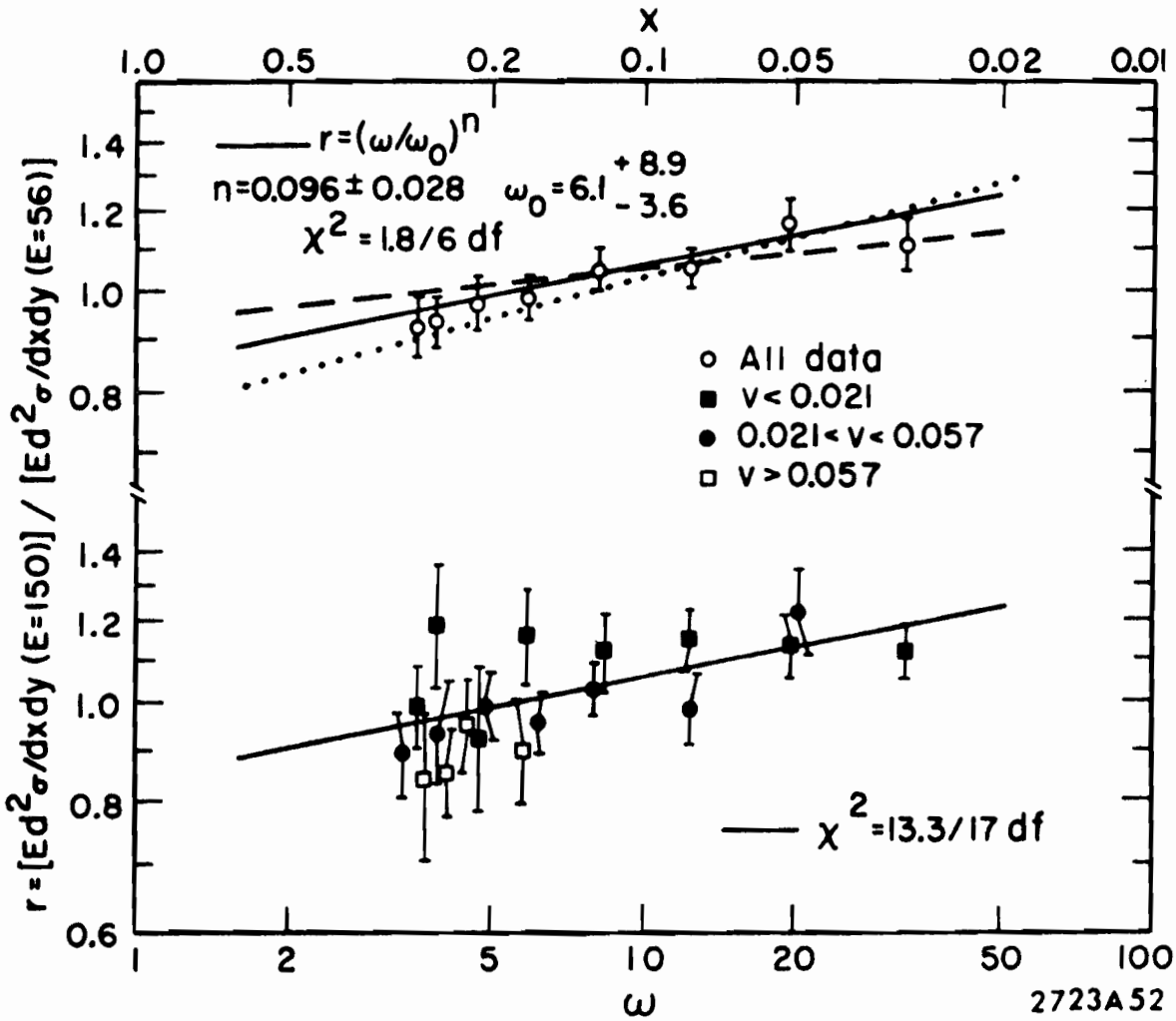
x
1.0
0.5
0.2
0.1
0.05
0.02
0.01
r=(ω/ω0)^n
n=0.096 ± 0.028
ω0=6.1 +8.9 -3.6
χ2 = 1.8/6 df
All data
v< 0.021
0.021< v< 0.057
v > 0.057
χ2=13.3/17 df
r=[Ed2σ/dxdy (E=150)] / [Ed2σ/dxdy (E=56)]
1.4
1.2
1.0
0.8
0.6
1
2
5
10
20
50
100
ω
2723A52

Figure 4

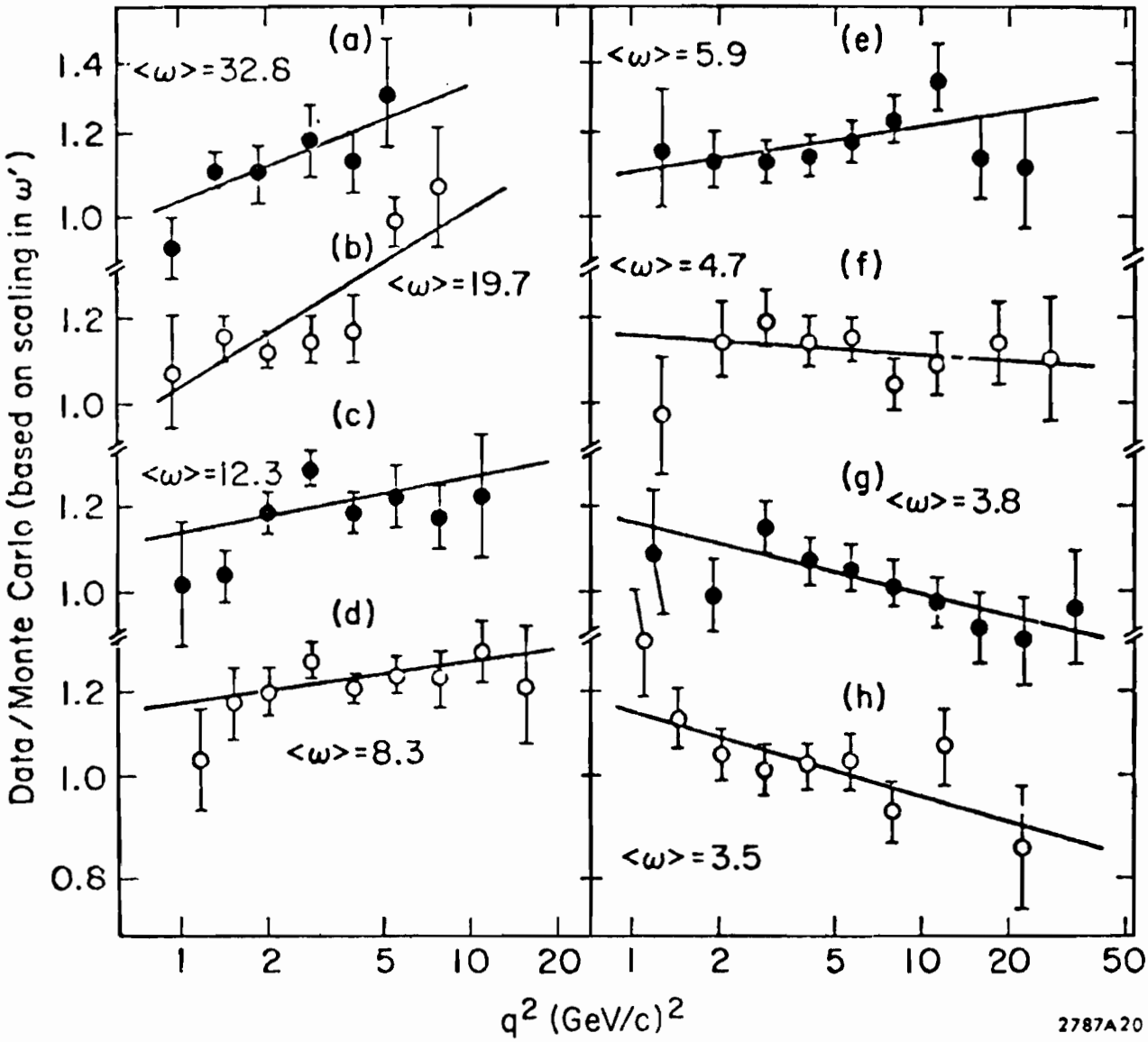
(a)
<ω>=32.8
(b)
<ω>=19.7
(c)
<ω>=12.3
(d)
<ω>=8.3
(e)
<ω>=5.9
(f)
<ω>=4.7
(g)
<ω>=3.8
(h)
<ω>=3.5
Data/Monte Carlo (based on scaling in ω')
q² (GeV/c)²
2787A20

Figure 5

FERMILAB-CONF-76-145-E

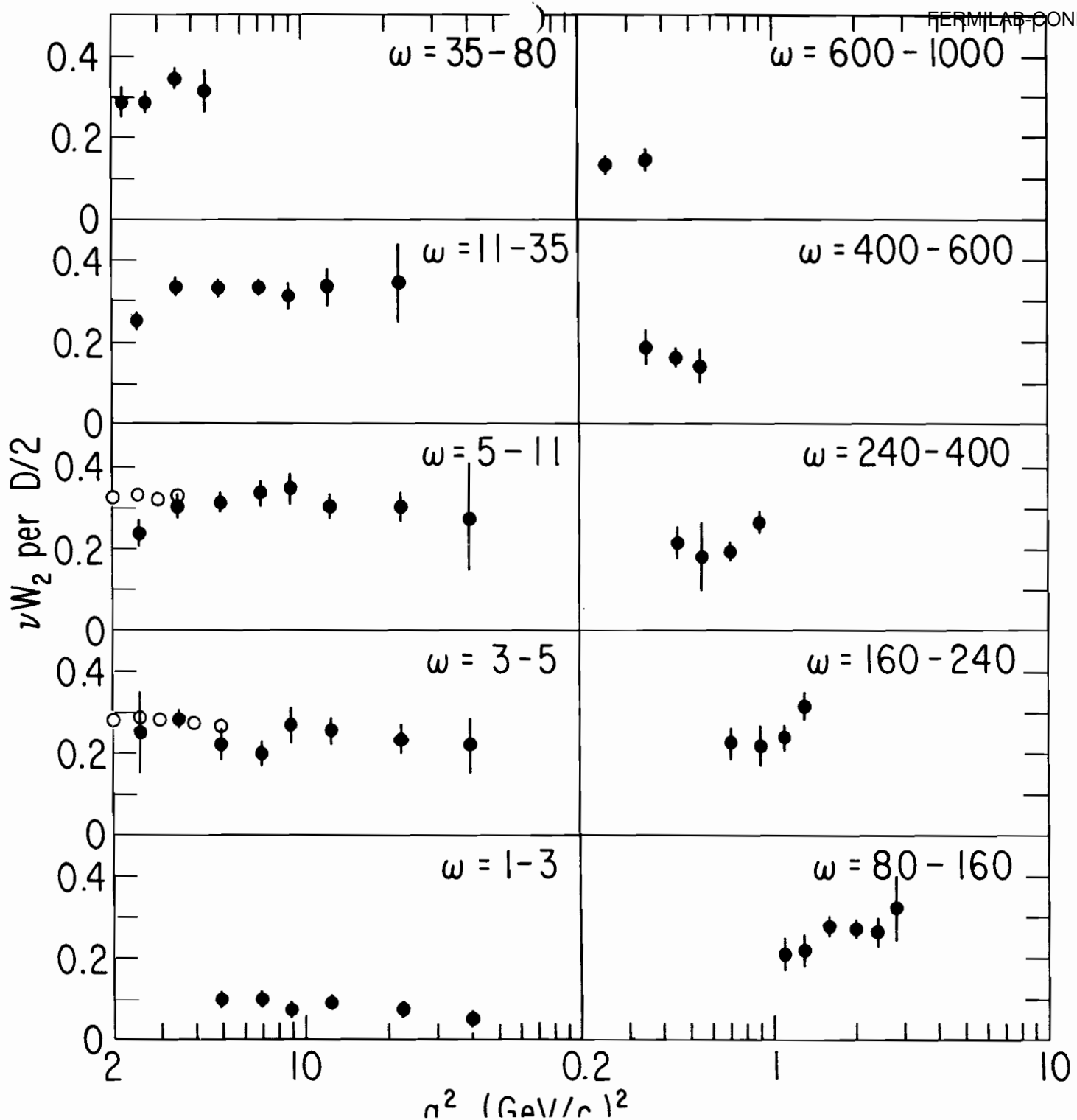

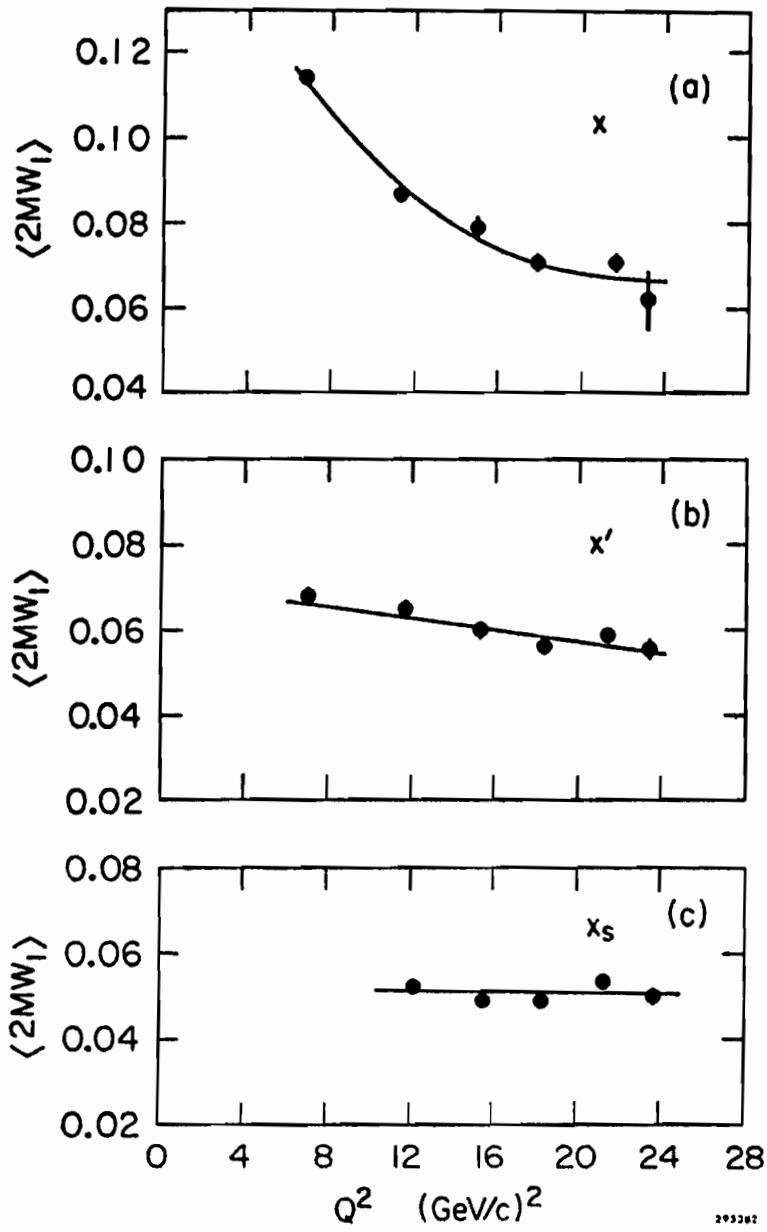
0.12
0.10
0.08
0.06
0.04
⟨2MW1⟩
(a)
x
0.10
0.08
0.06
0.04
0.02
⟨2MW1⟩
(b)
x′
0.08
0.06
0.04
0.02
⟨2MW1⟩
(c)
xs
0
4
8
12
16
20
24
28
Q2 (GeV/c)2

Figure 7

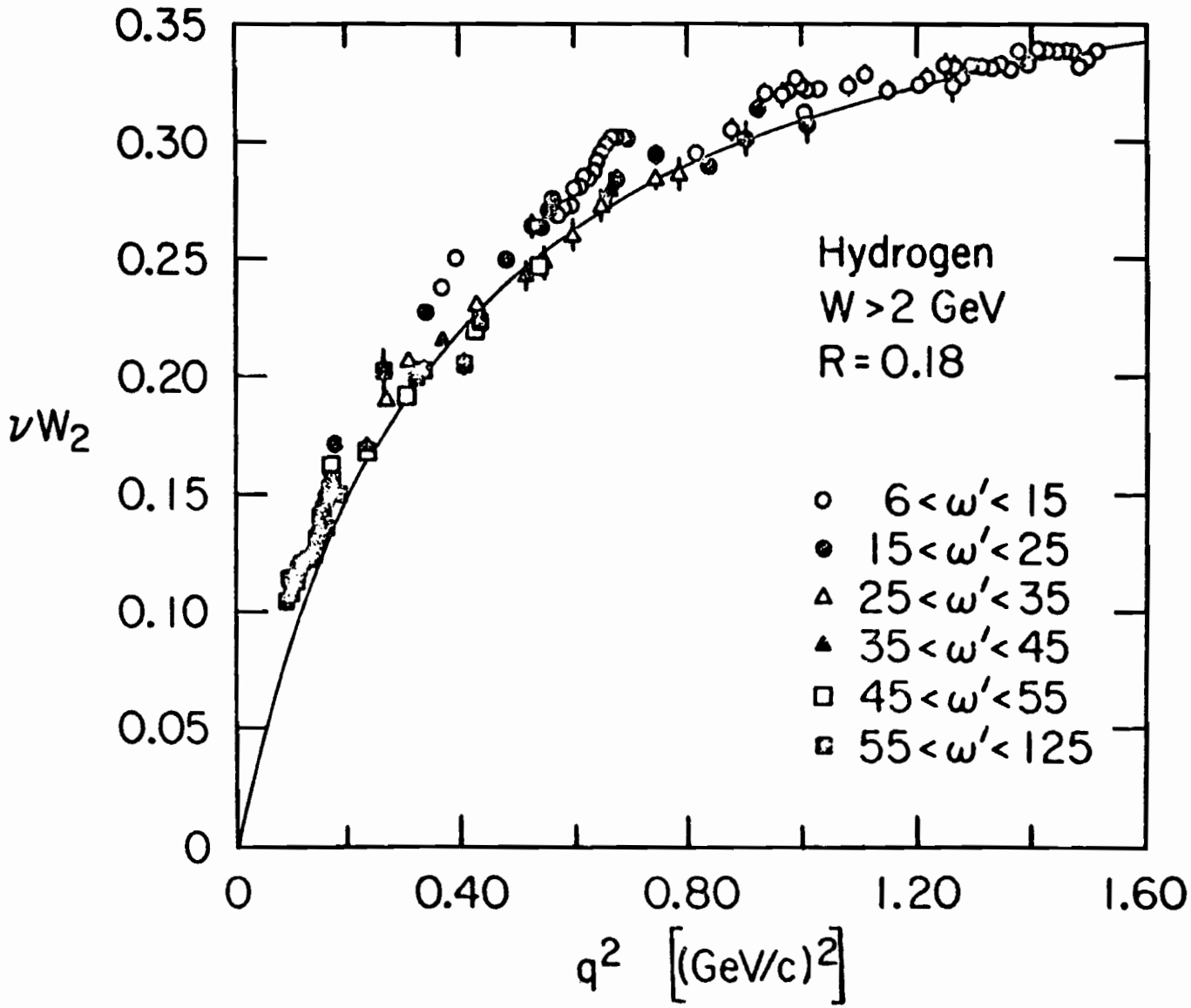
0.35
0.30
0.25
0.20
0.15
0.10
0.05
0
νW_2
0
0.40
0.80
1.20
1.60
q^2 [(GeV/c)^2]
Hydrogen
W > 2 GeV
R = 0.18
6 < ω′ < 15
15 < ω′ < 25
25 < ω′ < 35
35 < ω′ < 45
45 < ω′ < 55
55 < ω′ < 125

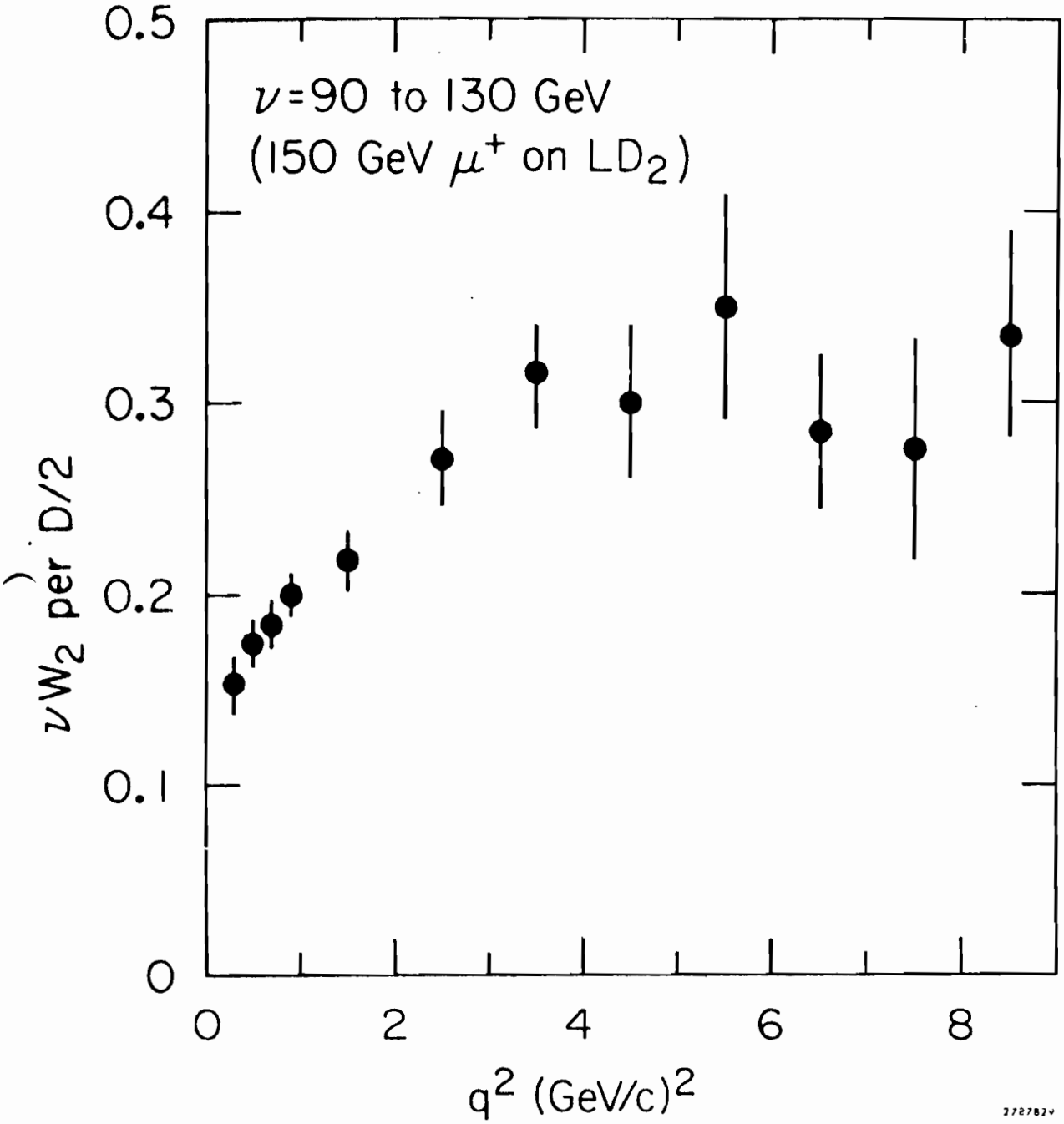
ν=90 to 130 GeV
(150 GeV μ^+ on LD_2)
0.5
0.4
0.3
0.2
0.1
0
νW_2 per D/2
0
2
4
6
8
q^2 (GeV/c)^2

Figure 9

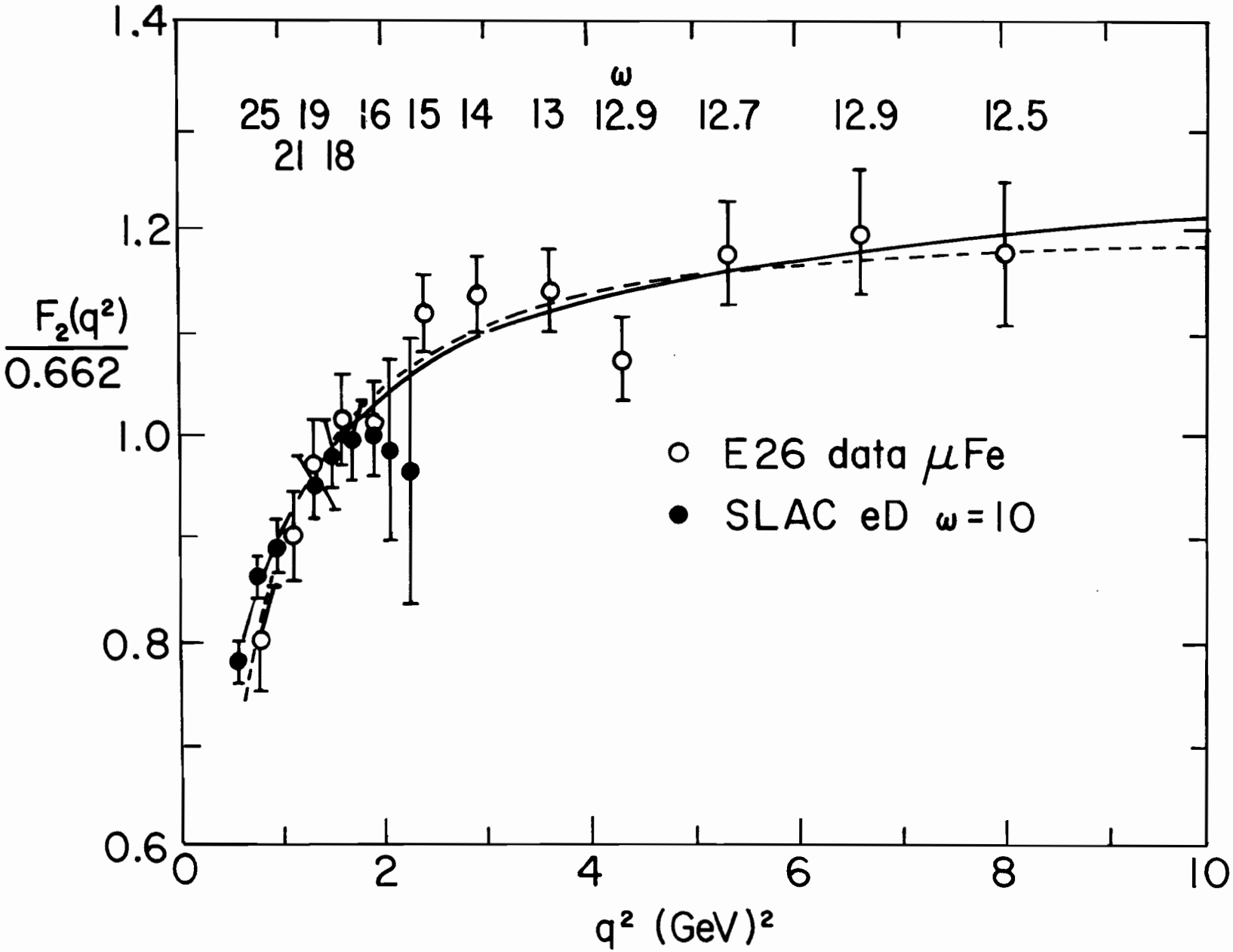
ω
25 19 16 15 14 13 12.9 12.7 12.9 12.5
21 18
1.4
1.2
1.0
0.8
0.6
$\frac{F_2(q^2)}{0.662}$
0
2
4
6
8
10
q^2 (GeV)^2
E26 data μFe
SLAC eD $\omega = 10$

Figure 10

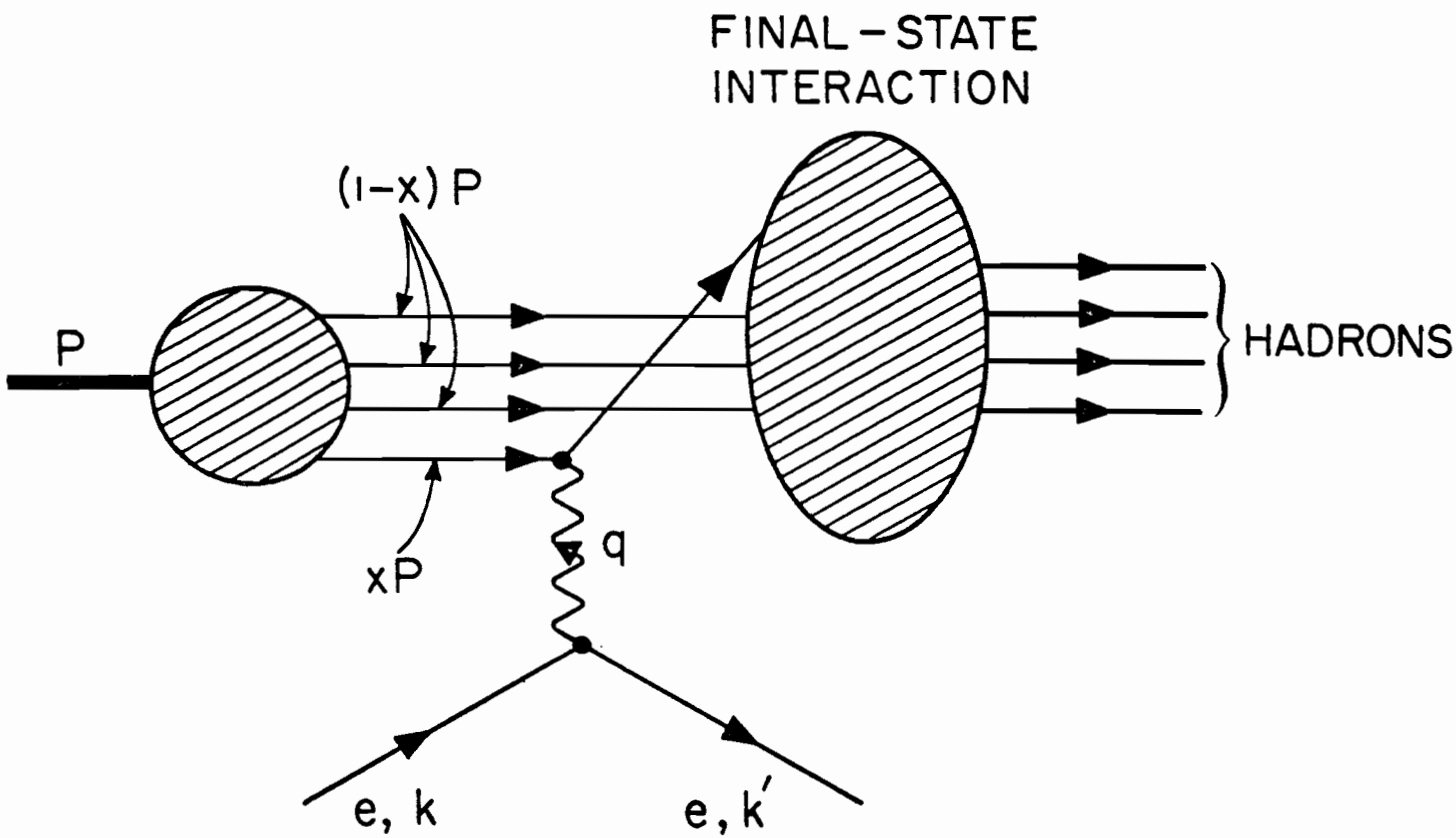

Figure 11

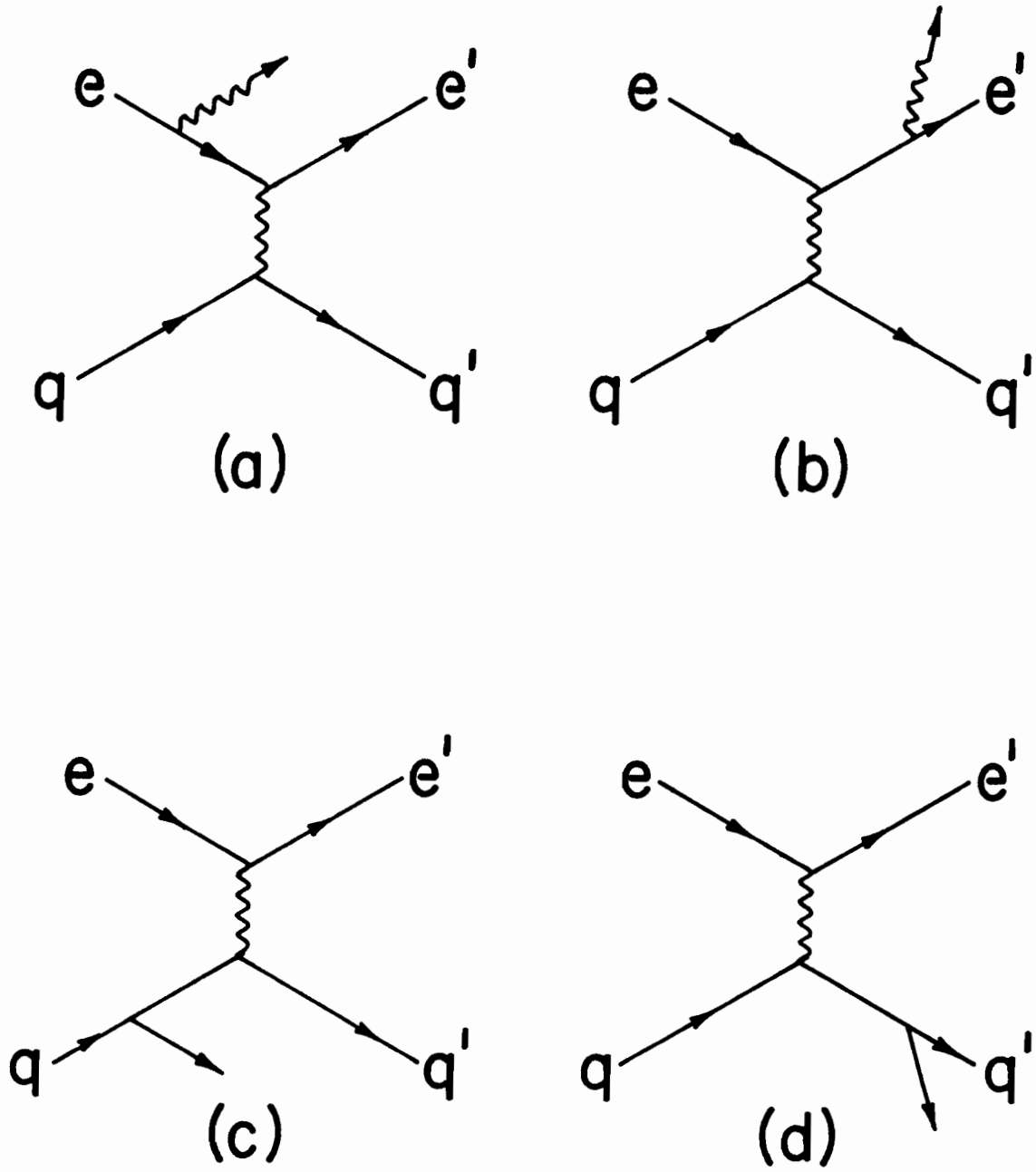

Figure 12

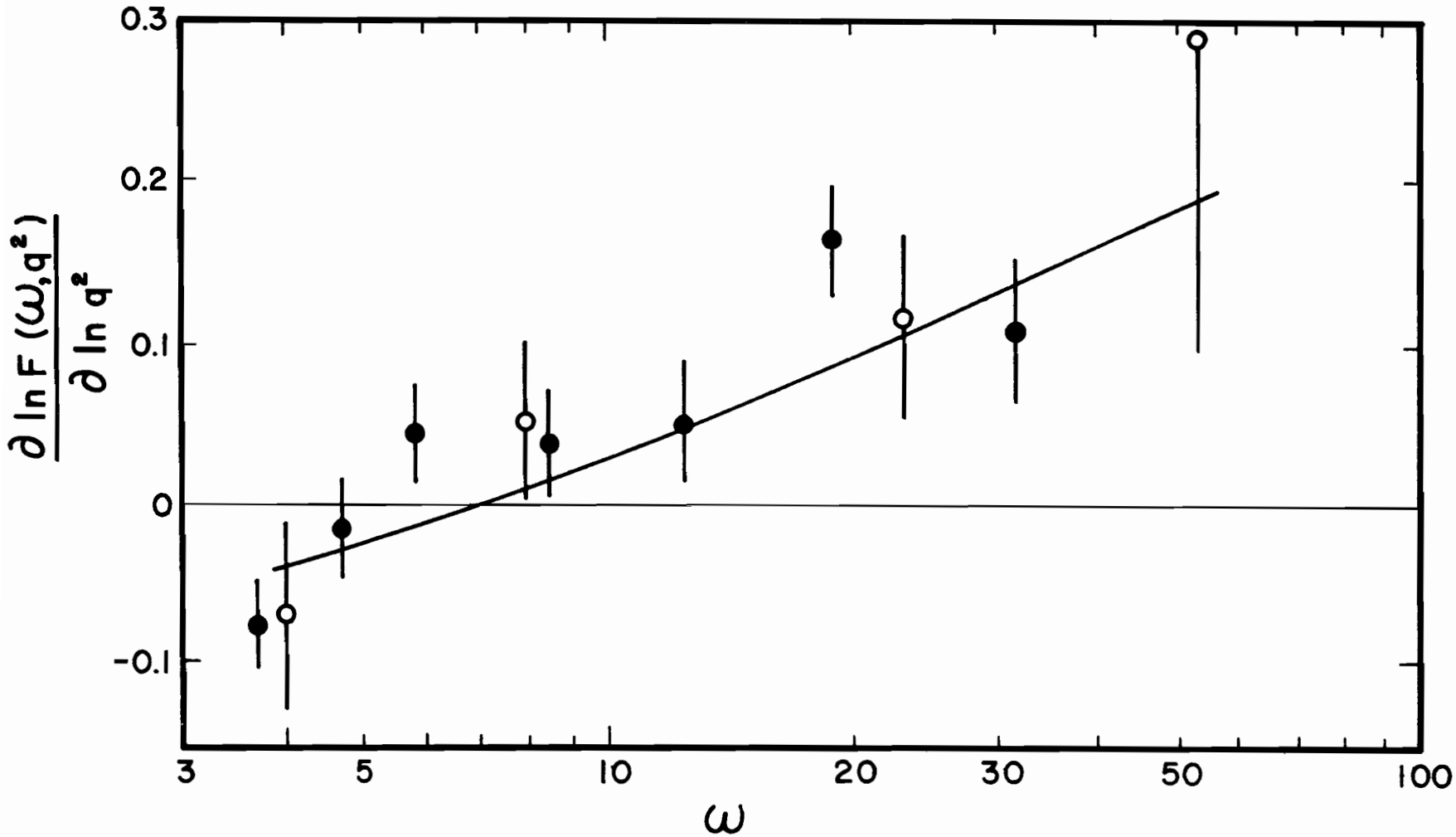
0.3
0.2
0.1
0
-0.1
$\frac{\partial \ln F(\omega, q^2)}{\partial \ln q^2}$
3
5
10
20
30
50
100
ω

Figure 13

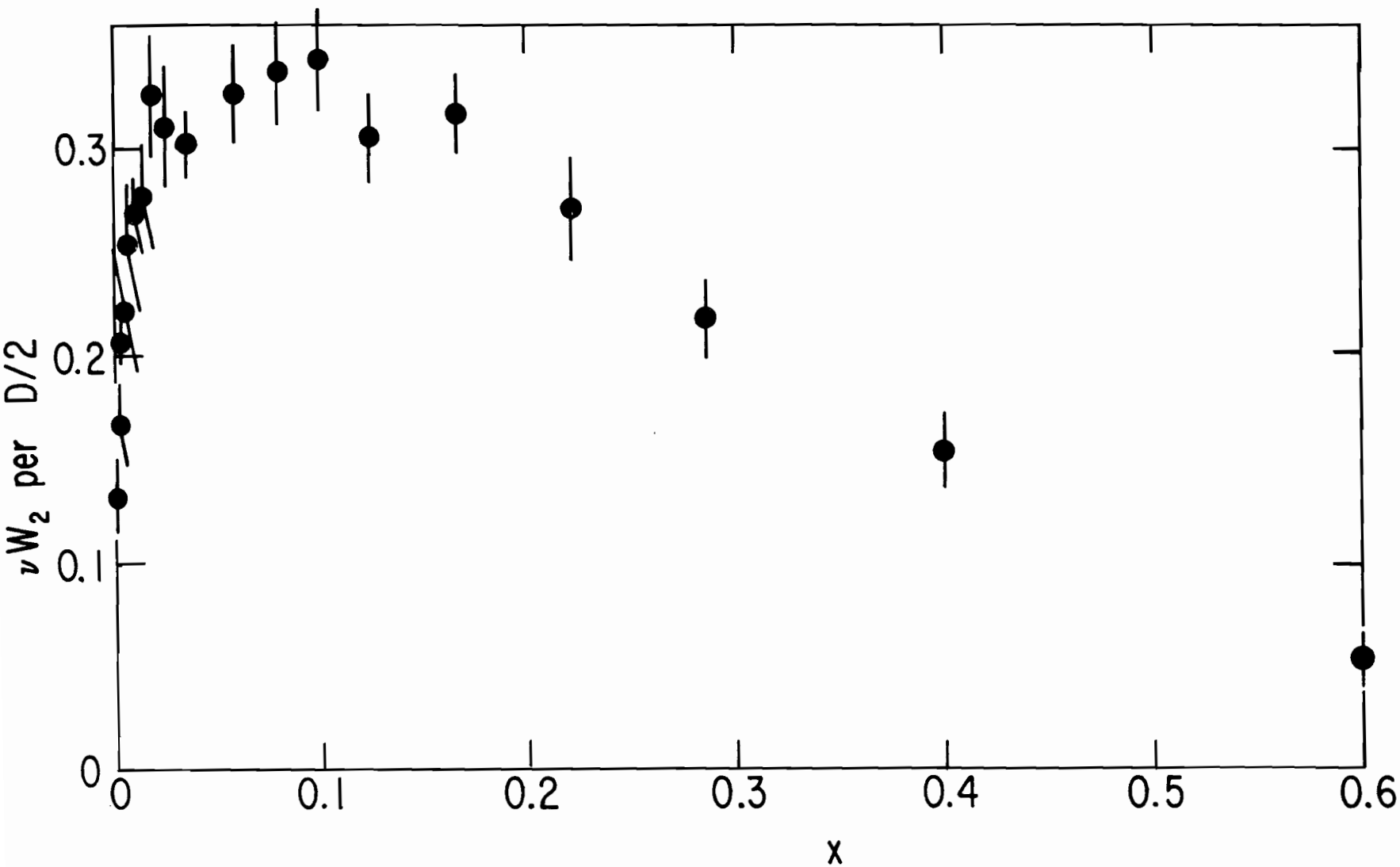

Figure 14

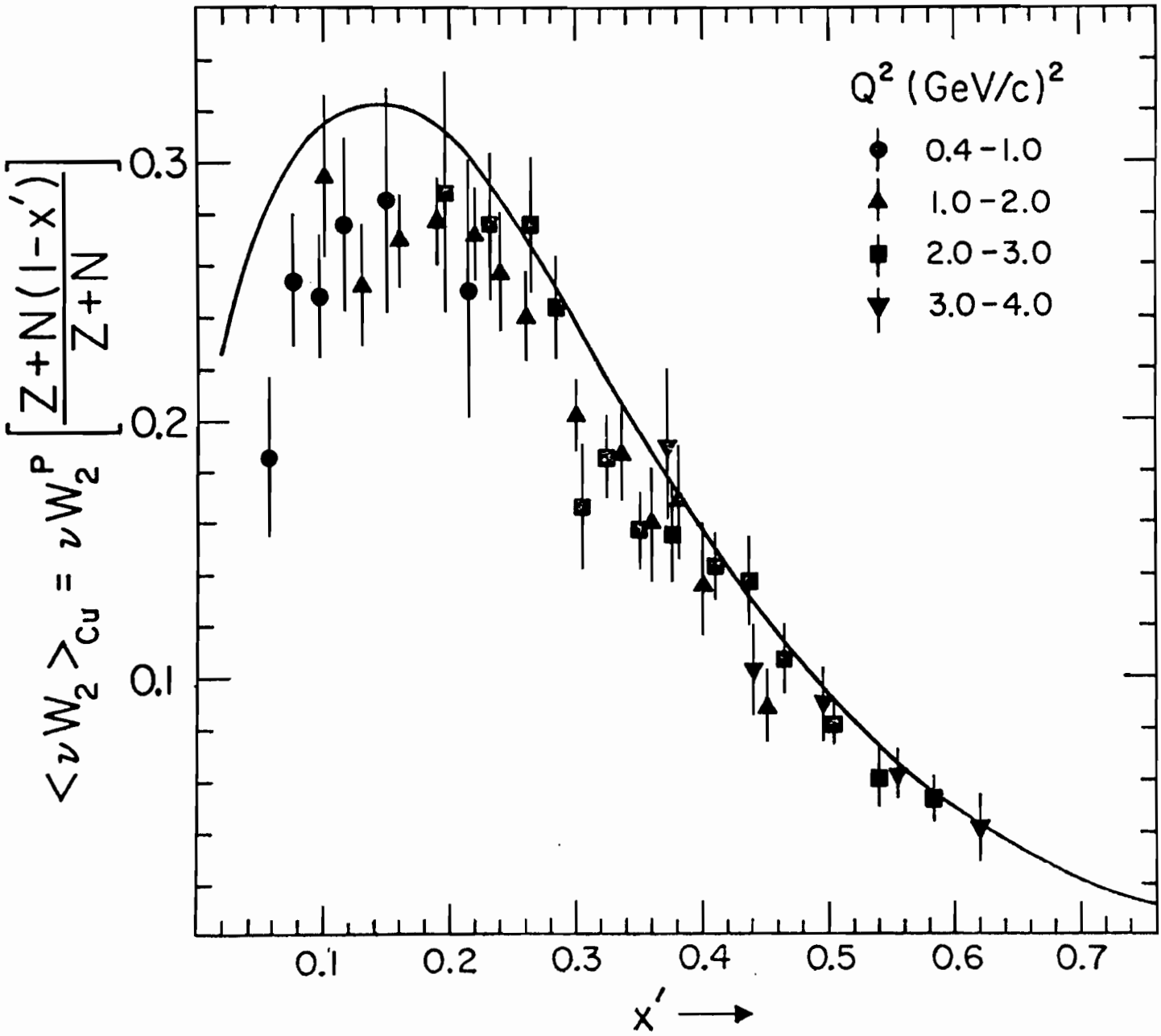
Q^2 (GeV/c)^2
0.4 - 1.0
1.0 - 2.0
2.0 - 3.0
3.0 - 4.0
$\langle \nu W_2 \rangle_{Cu} = \nu W_2^p \left[\frac{Z+N(1-x')}{Z+N}\right]$
0.3
0.2
0.1
0.1
0.2
0.3
0.4
0.5
0.6
0.7
$x' \longrightarrow$

Figure 15

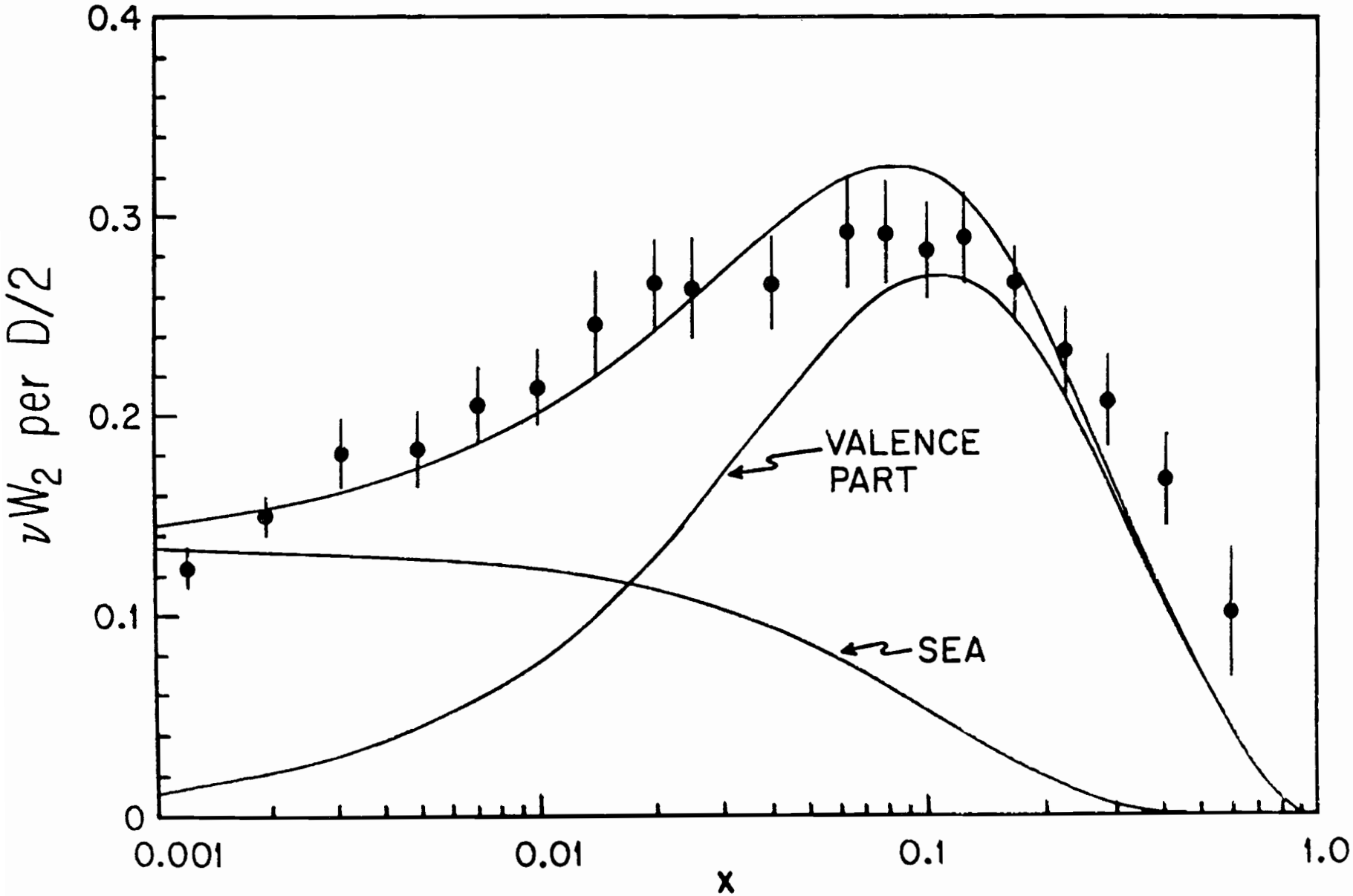

Figure 16

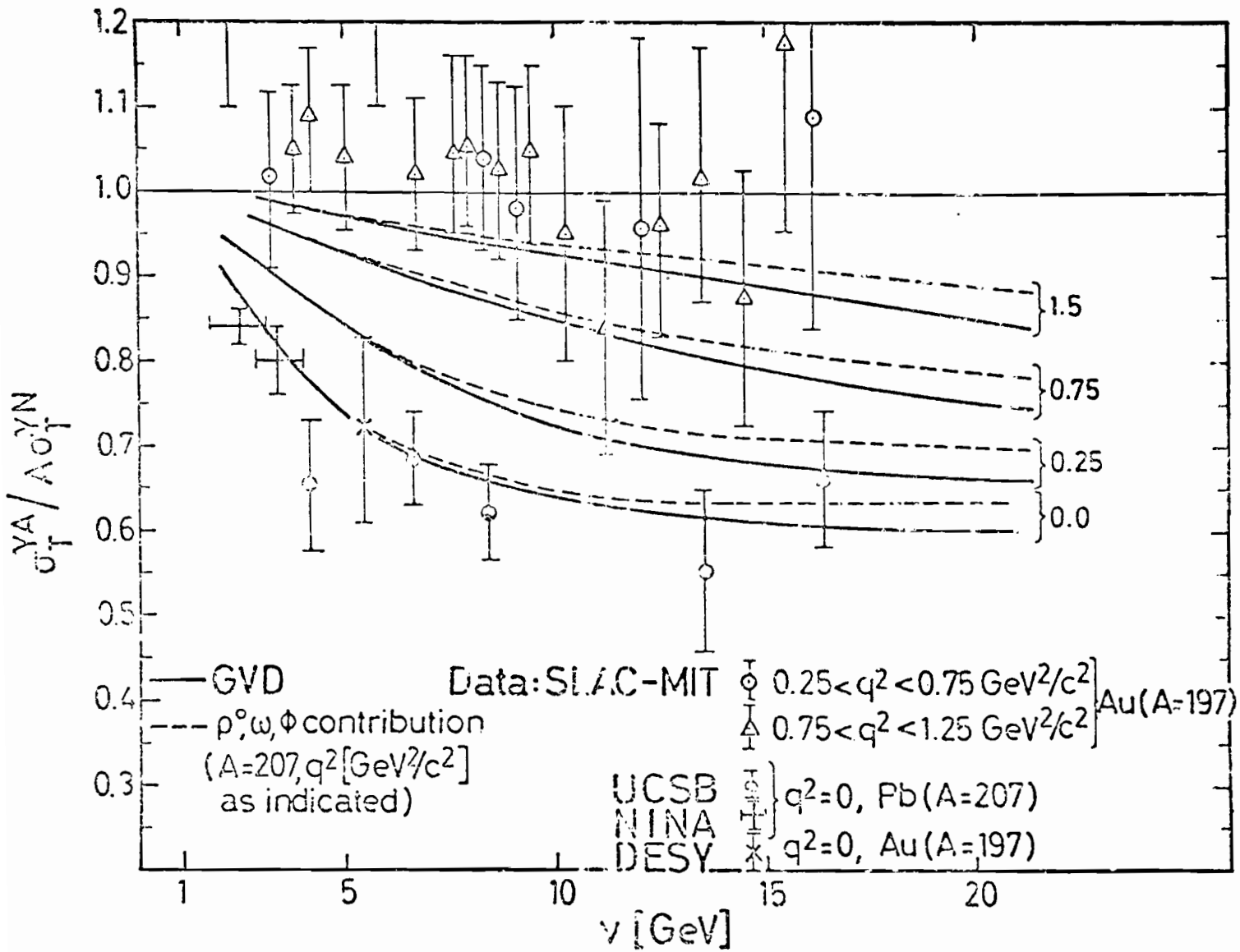
1.2
1.1
1.0
0.9
0.8
0.7
0.6
0.5
0.4
0.3
$\sigma_T^{\gamma A} / A\sigma_T^{\gamma N}$
1.5
0.75
0.25
0.0
GVD
ρ°,ω,Φ contribution
(A=207, q²[GeV²/c²]
as indicated)
Data: SLAC-MIT
0.25<q²<0.75 GeV²/c²
0.75<q²<1.25 GeV²/c²
Au(A=197)
UCSB
NINA
q²=0, Pb(A=207)
DESY
q²=0, Au(A=197)
1
5
10
15
20
ν [GeV]

Figure 17

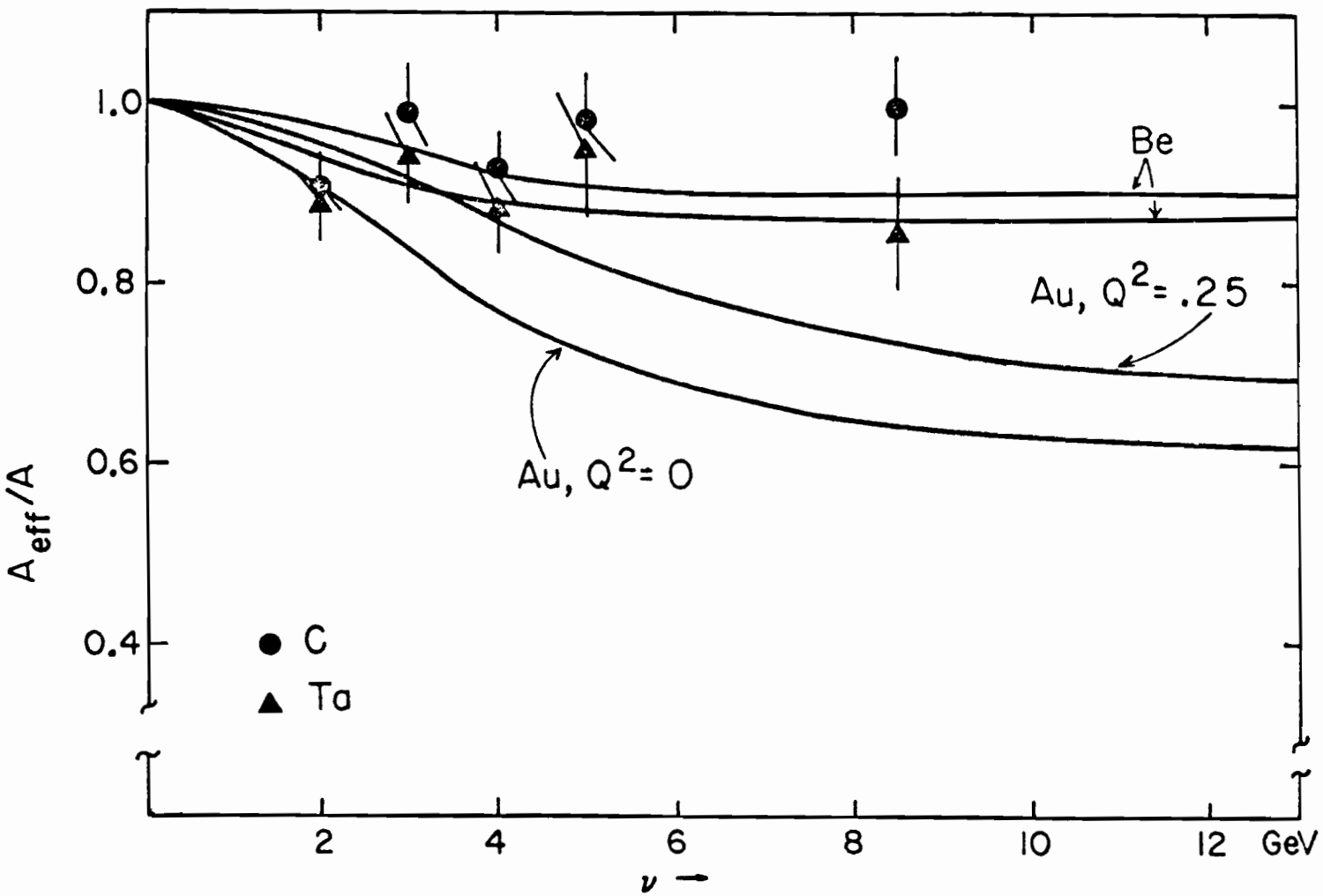

Figure 18

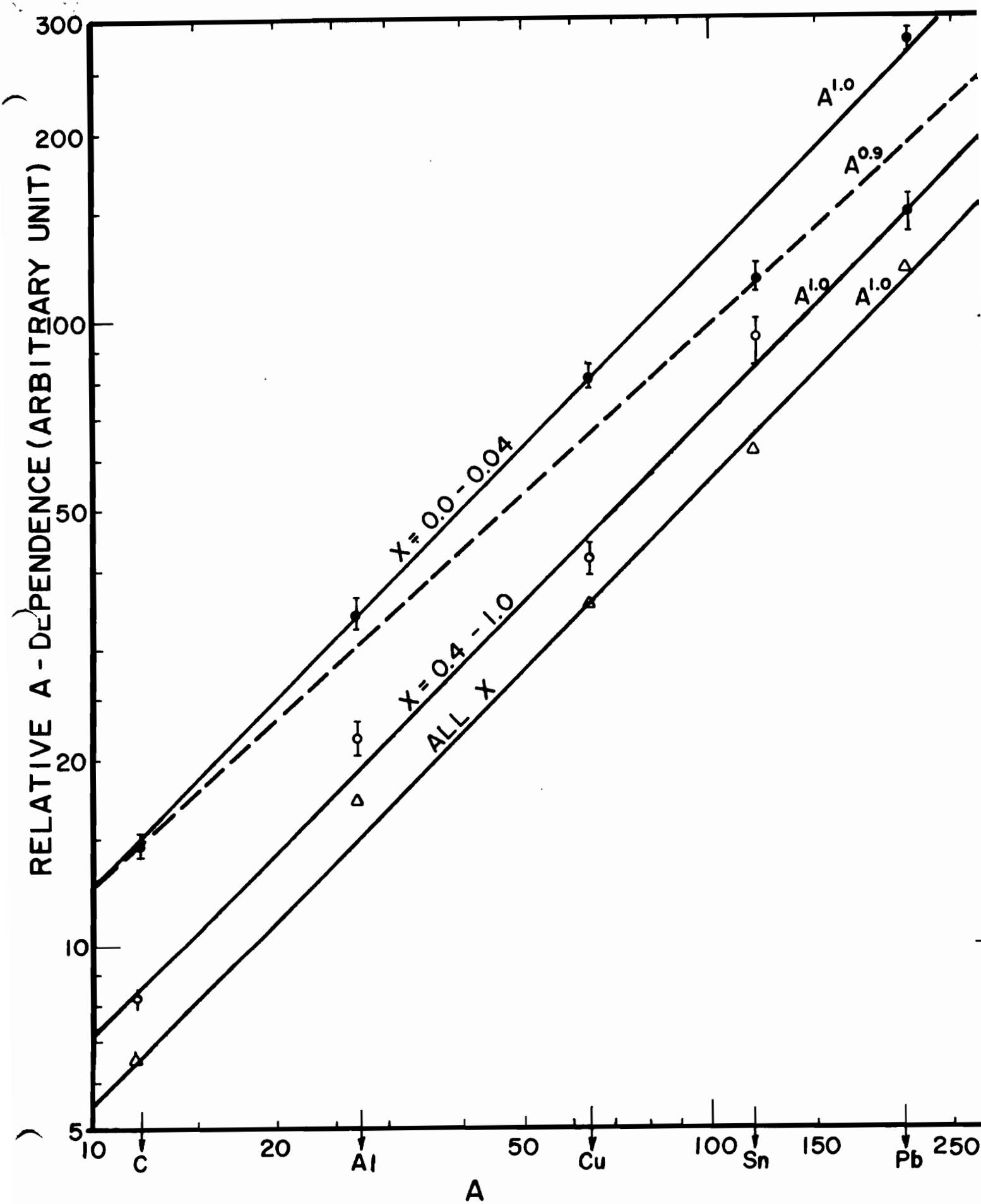
RELATIVE A - DEPENDENCE (ARBITRARY UNIT)
300
200
100
50
20
10
5
10
20
50
100
150
250
C
Al
Cu
Sn
Pb
A
$A^{1.0}$
$A^{0.9}$
$A^{1.0}$
$A^{1.0}$
X = 0.0 - 0.04
X = 0.4 - 1.0
ALL X

Figure 19

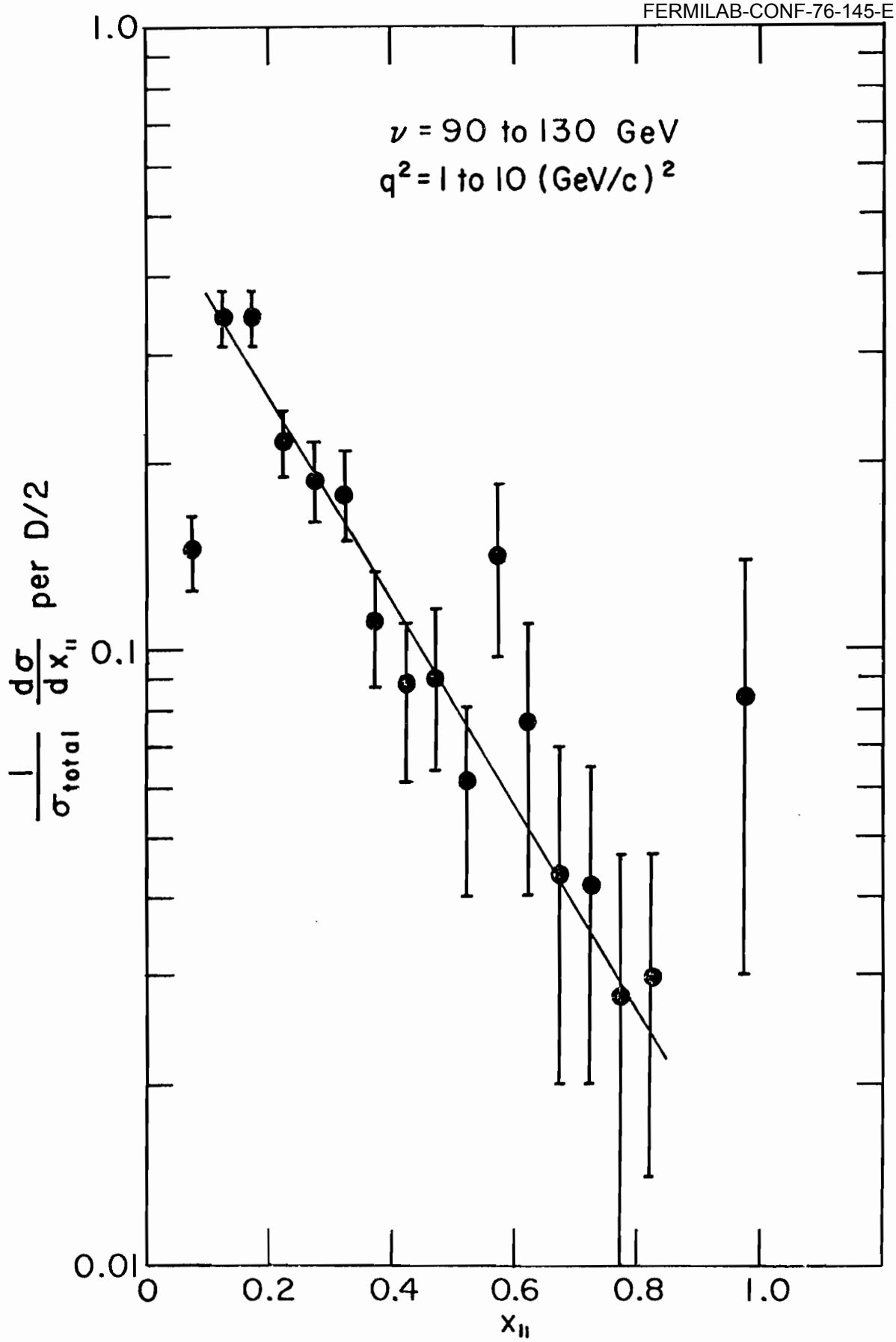
ν = 90 to 130 GeV
q^2 = 1 to 10 (GeV/c)^2
$\frac{1}{\sigma_{total}} \frac{d\sigma}{dx_{\parallel}}$ per D/2
1.0
0.1
0.01
0
0.2
0.4
0.6
0.8
1.0
$x_{\parallel}$

Figure 20

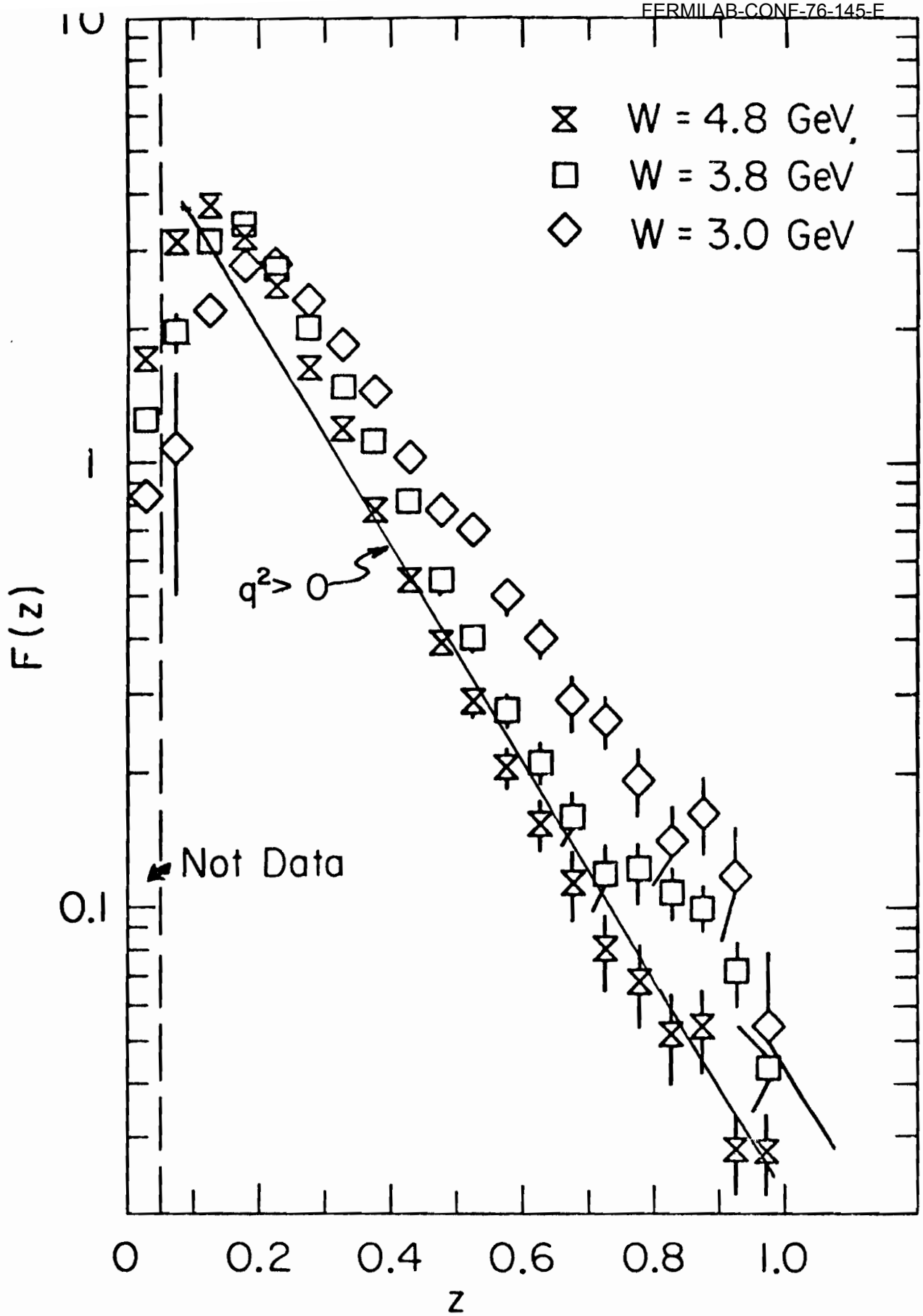

Figure 21

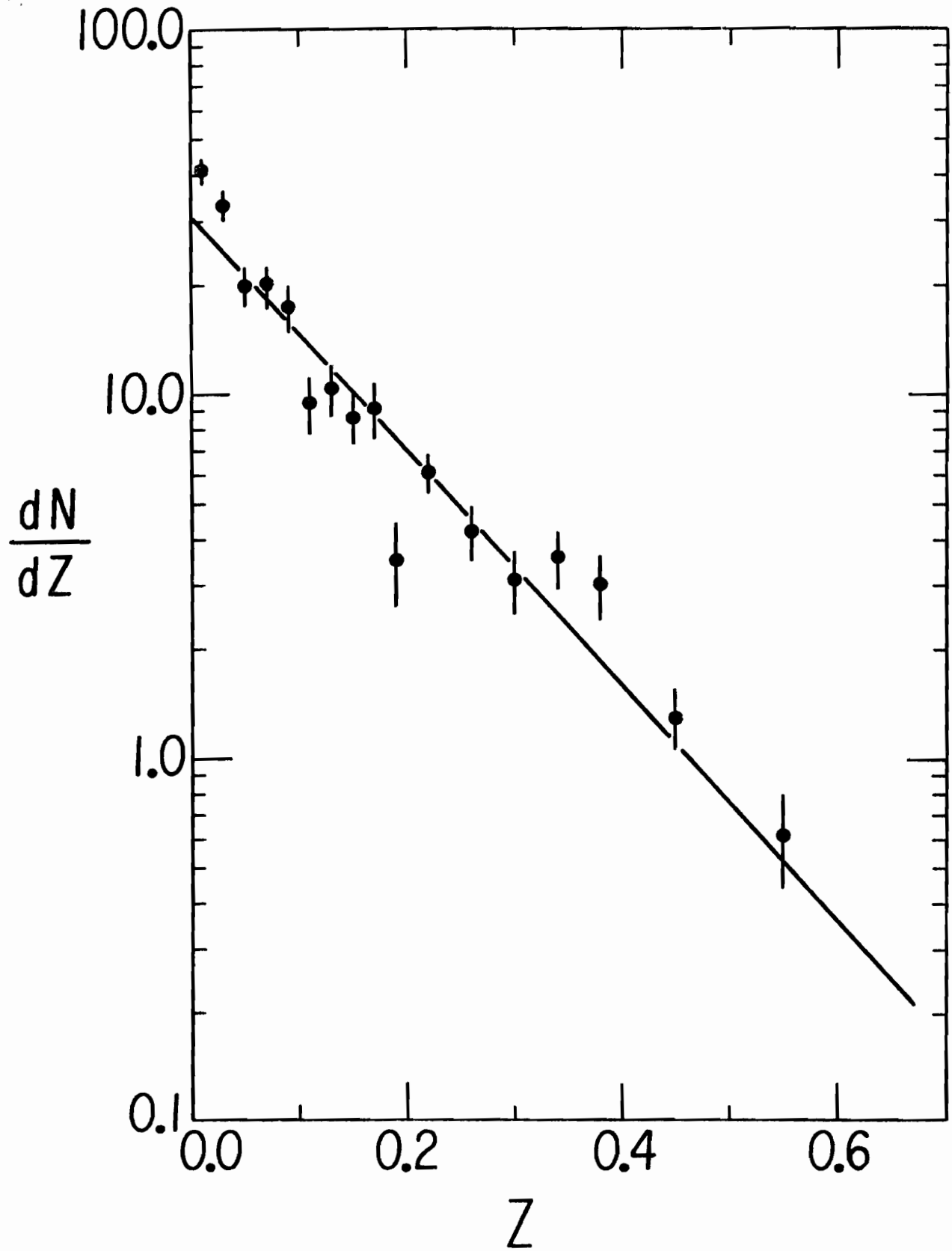

Figure 22

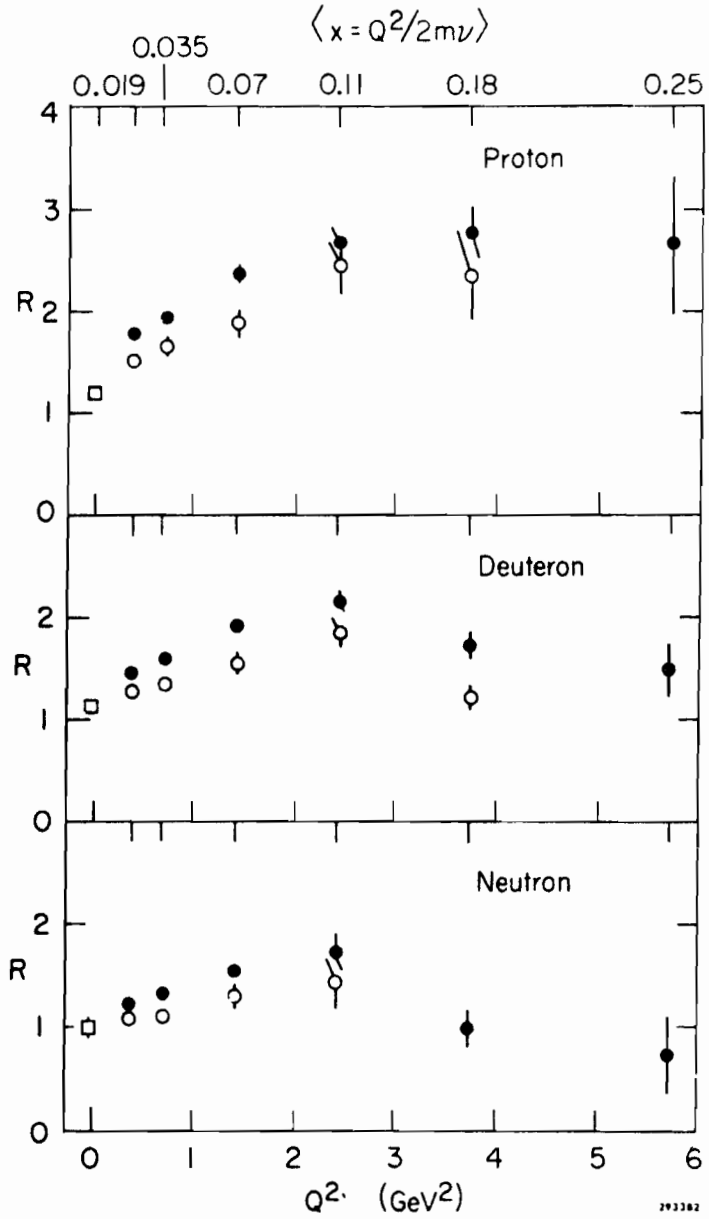
⟨x = Q²/2mν⟩
0.035
0.019
0.07
0.11
0.18
0.25
Proton
Deuteron
Neutron
R
Q² (GeV²)

Figure 23

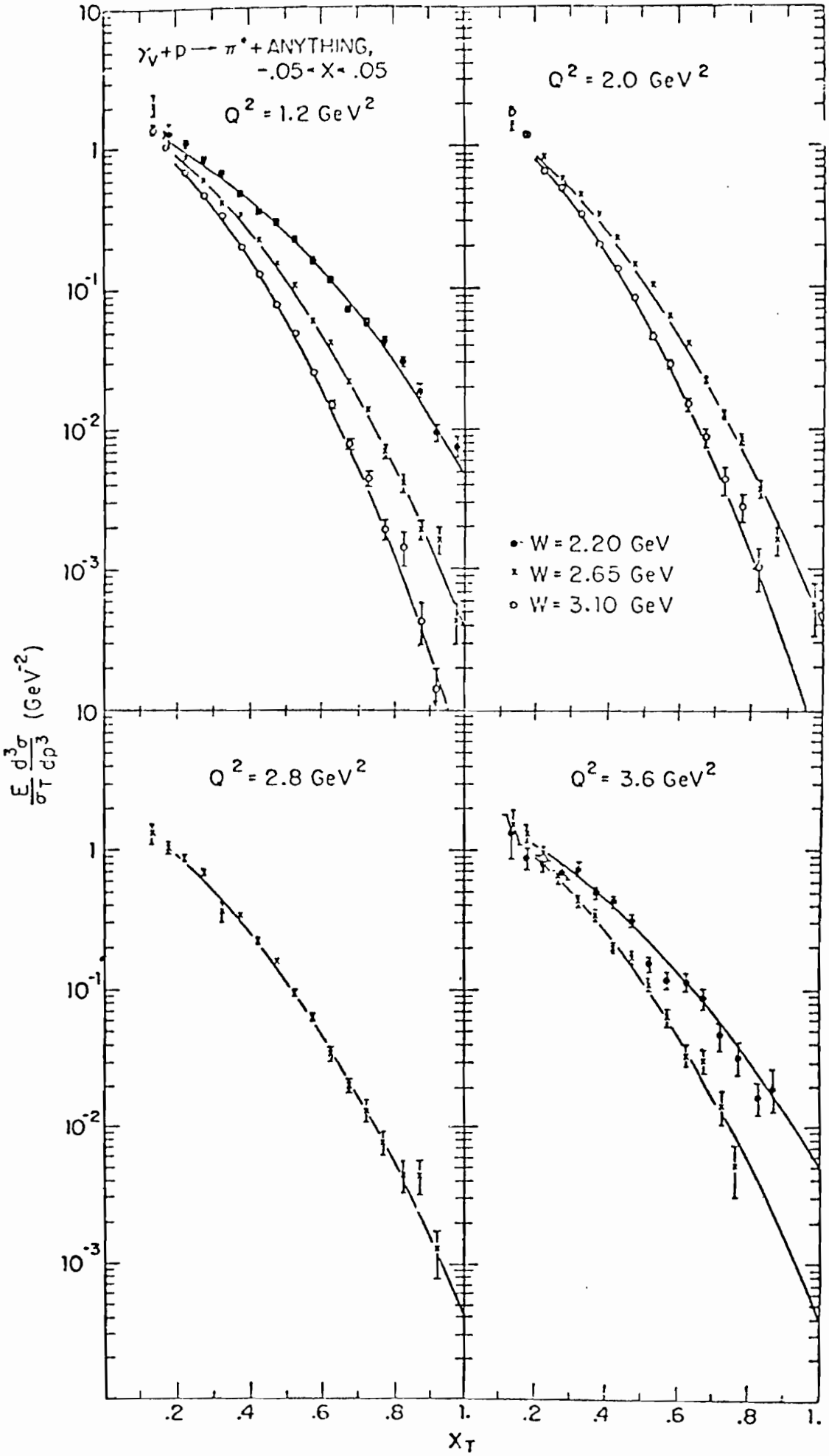
$\gamma_V + p \rightarrow \pi^+ + \text{ANYTHING}$,
$-.05 < X < .05$
$Q^2 = 1.2\ \text{GeV}^2$
$Q^2 = 2.0\ \text{GeV}^2$
$Q^2 = 2.8\ \text{GeV}^2$
$Q^2 = 3.6\ \text{GeV}^2$
• W = 2.20 GeV
x W = 2.65 GeV
o W = 3.10 GeV
$\frac{E}{\sigma_T}\frac{d^3\sigma}{dp^3}$ (GeV^{-2})
X_T

Figure

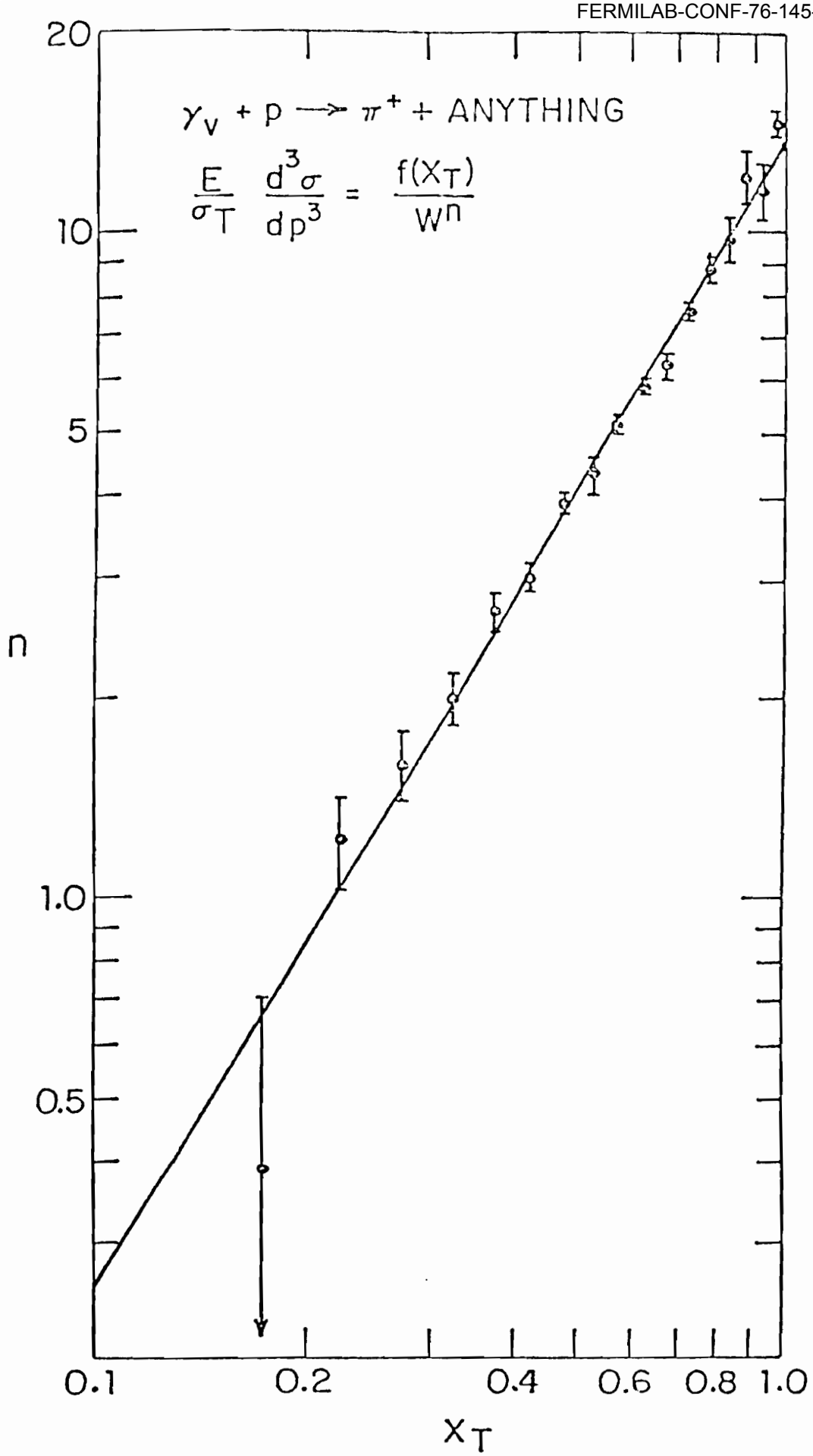
$\gamma_V + p \rightarrow \pi^+ + \text{ANYTHING}$
$\frac{E}{\sigma_T} \frac{d^3\sigma}{dp^3} = \frac{f(X_T)}{W^n}$
20
10
5
1.0
0.5
n
0.1
0.2
0.4
0.6
0.8
1.0
X_T

Figure 25

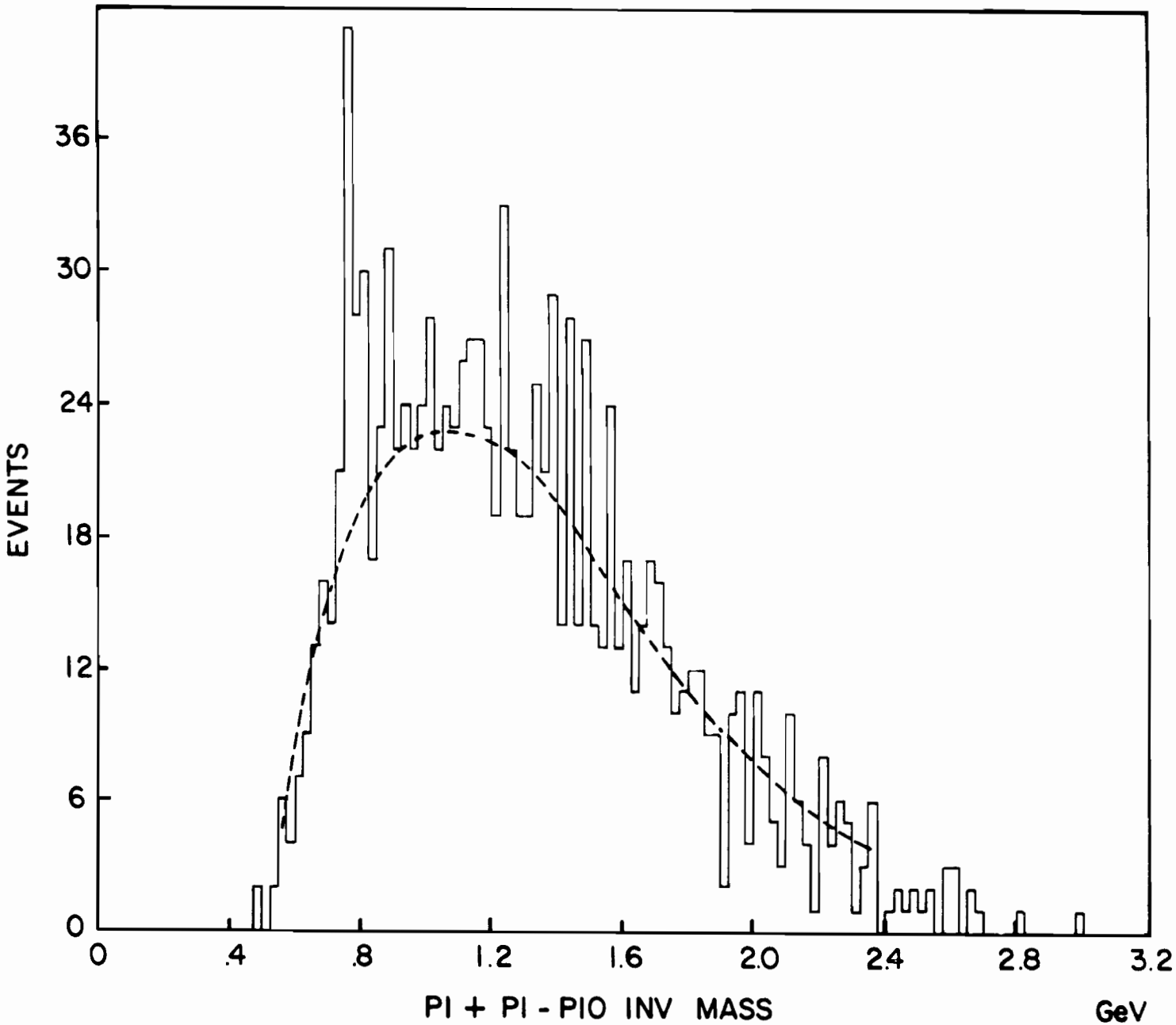
EVENTS
36
30
24
18
12
6
0
0
.4
.8
1.2
1.6
2.0
2.4
2.8
3.2
PI + PI - PIO INV MASS
GeV

Figure 26

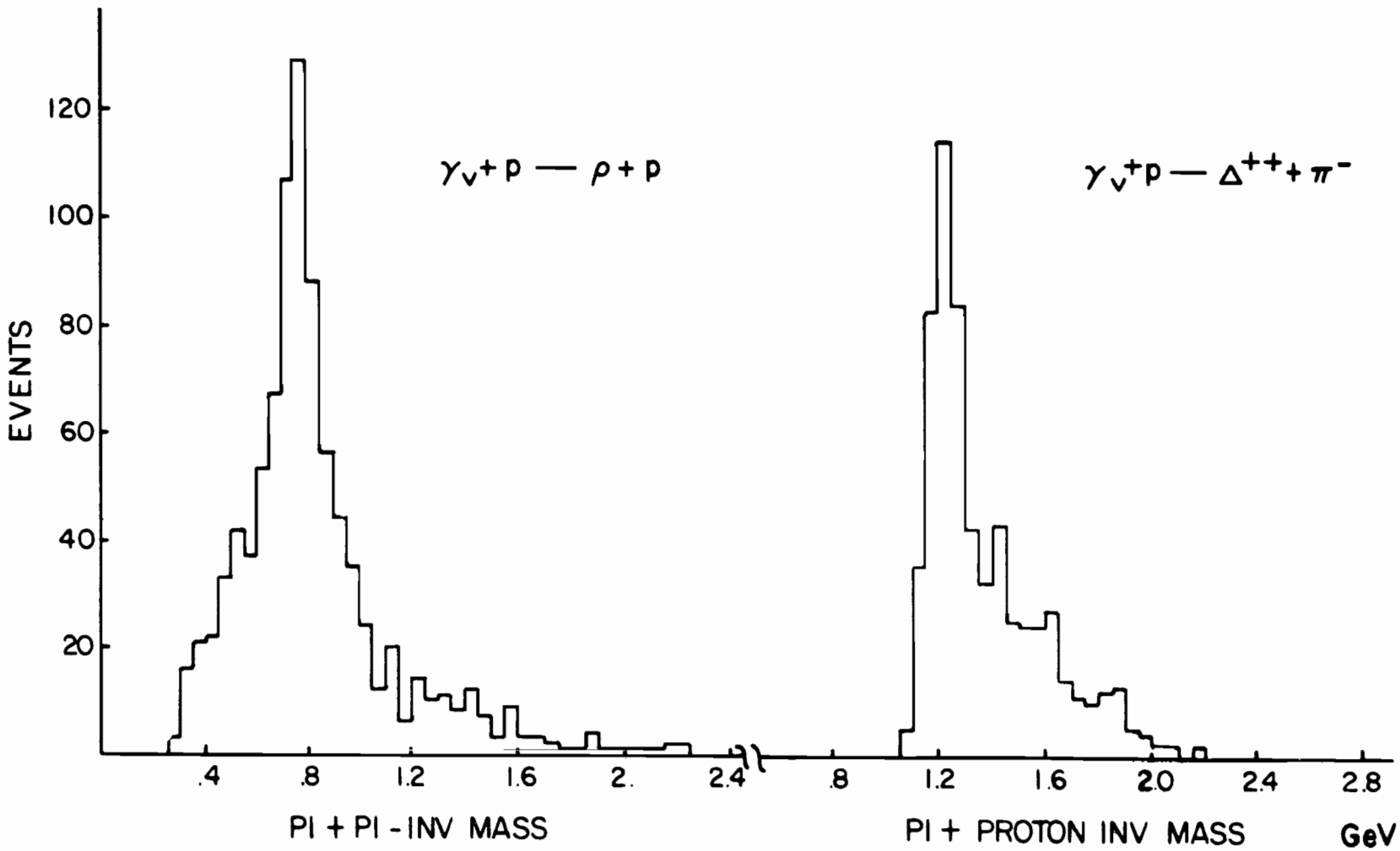

INVARIANT MASS DISTRIBUTION OF $\pi^+\pi^-$ AND π^+p FOR 4C, 4 PRONG EVENTS SHOWING A PEAK AT THE Δ^{++} AND THE ρ

Figure 27

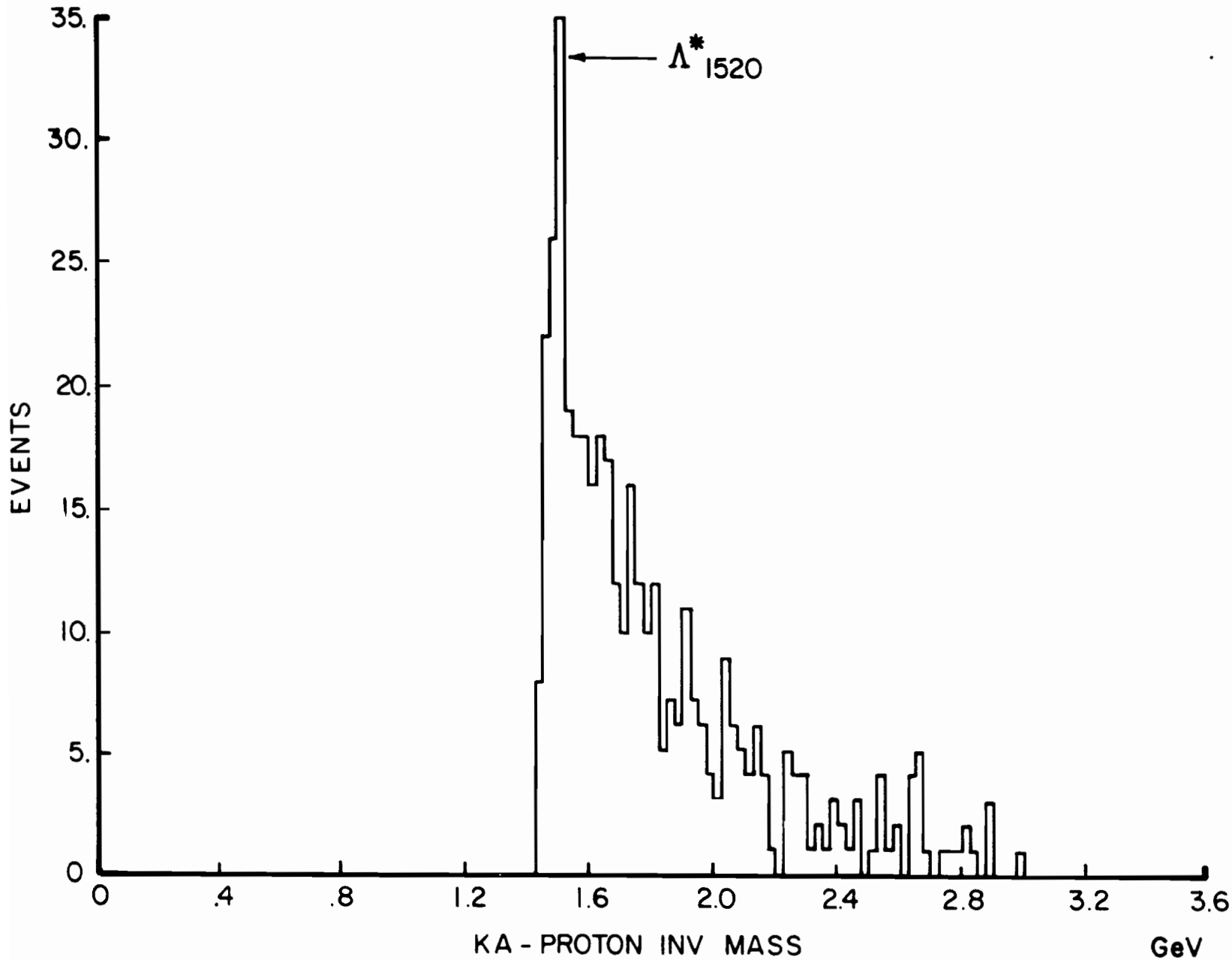
35.
30.
25.
20.
15.
10.
5.
0
EVENTS
Λ^*_{1520}
0
.4
.8
1.2
1.6
2.0
2.4
2.8
3.2
3.6
KA - PROTON INV MASS
GeV

Figure 28

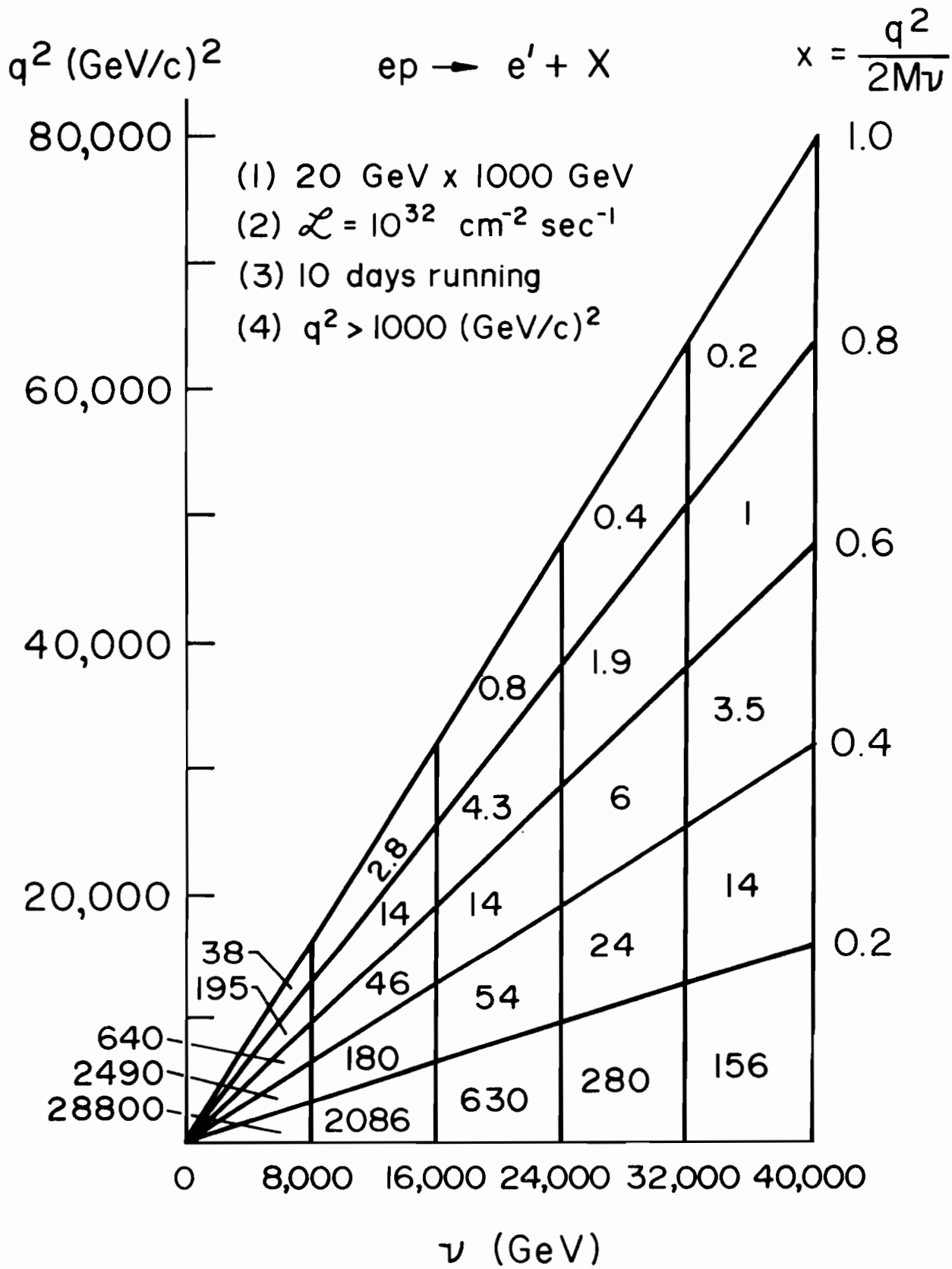
q^2 (GeV/c)^2
ep → e′ + X
$x = \frac{q^2}{2M\nu}$
80,000
60,000
40,000
20,000
(1) 20 GeV x 1000 GeV
(2) $\mathcal{L} = 10^{32}$ cm^{-2} sec^{-1}
(3) 10 days running
(4) $q^2 > 1000$ (GeV/c)^2
1.0
0.8
0.6
0.4
0.2
0.2
0.4
1
0.8
1.9
3.5
2.8
4.3
6
14
14
14
24
38
195
46
54
640
180
2490
28800
2086
630
280
156
0
8,000
16,000
24,000
32,000
40,000
ν (GeV)

Figure 29

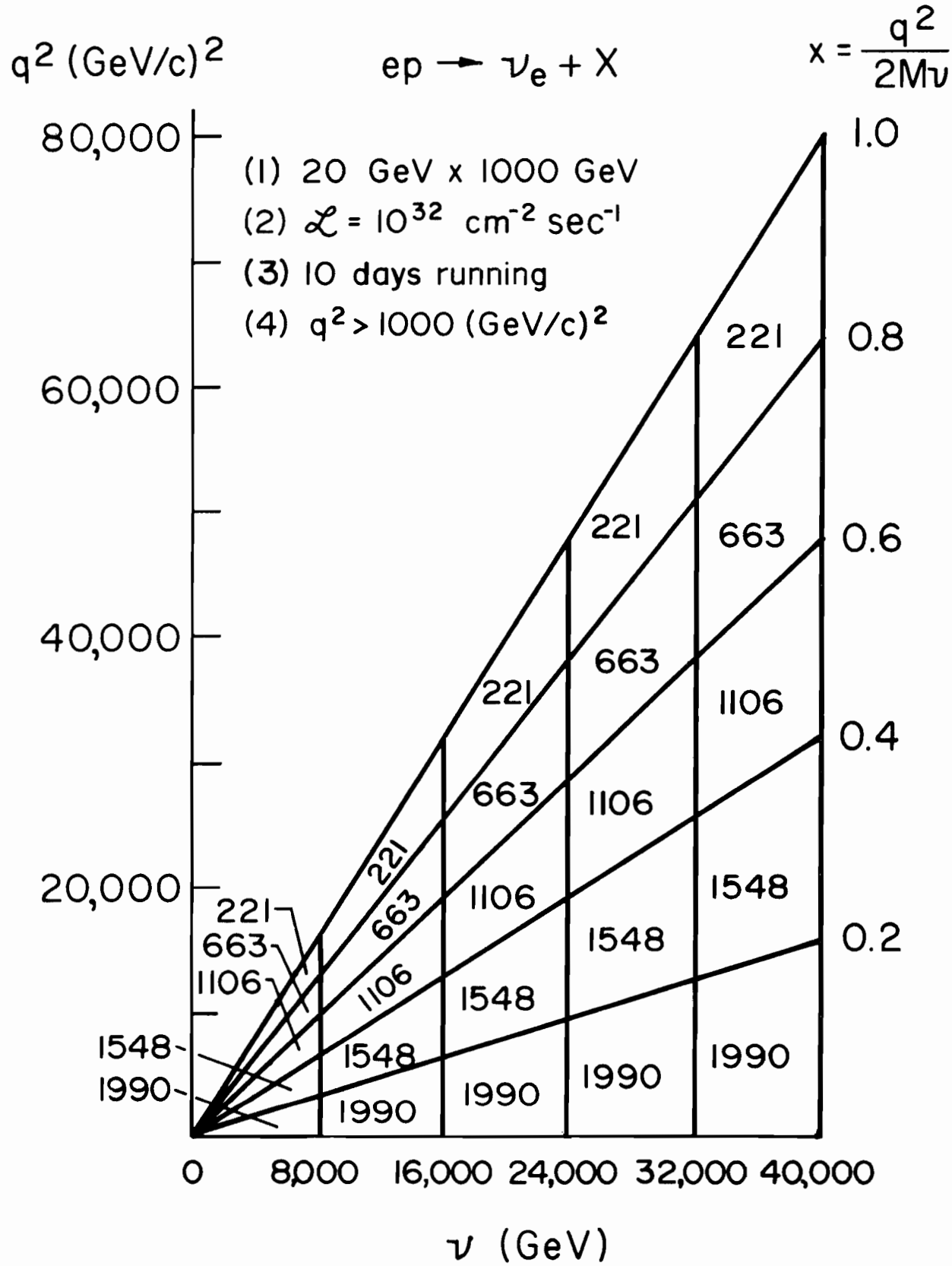
q2 (GeV/c)2
ep → νe + X
x = q2/2Mν
80,000
60,000
40,000
20,000
(1) 20 GeV x 1000 GeV
(2) ℒ = 10^32 cm^-2 sec^-1
(3) 10 days running
(4) q2 > 1000 (GeV/c)2
1.0
0.8
0.6
0.4
0.2
221
663
1106
1548
1990
0
8,000
16,000
24,000
32,000
40,000
ν (GeV)

Figure 30